Collaborative Multi-sensing in Energy Harvesting Wireless Sensor Networks

Vini Gupta, *Student Member, IEEE,* and Swades De, *Senior Member, IEEE*

***Abstract*—This paper presents an adaptive multi-sensing (MS) framework for a network of densely deployed solar energy harvesting wireless nodes. Each node is mounted with heterogeneous sensors to sense multiple cross-correlated slowly-varying parameters/signals. Inherent spatio-temporal correlations of the observed parameters are exploited to adaptively activate a subset of sensors of a few nodes and turn-OFF the remaining ones. To do so, a multi-objective optimization problem that jointly optimizes sensing quality and network energy efficiency is solved for each monitoring parameter. To increase energy efficiency, network and node-level collaborations based multi-sensing strategies are proposed. The former one utilizes spatial proximity (SP) of nodes with active sensors (obtained from the MS) to further reduce the active sensors sets, while the latter one exploits cross-correlation (CC) among the observed parameters at each node to do so. A retraining logic is developed to prevent deterioration of sensing quality in MS-SP. For jointly estimating all the parameters across the field nodes using under-sampled measurements obtained from MS-CC based active sensors, a multi-sensor data fusion technique is presented. For this ill-posed estimation scenario, double sparsity due to spatial and cross-correlation among measurements is used to derive principal component analysis-based Kronecker sparsifying basis, and sparse Bayesian learning framework is then used for joint sparse estimation. Extensive simulation studies using synthetic (real) data illustrate that, the proposed MS-SP and MS-CC strategies are respectively $48.2\ (52.09)\%$ and $50.30\ (8.13)\%$ more energy-efficient compared to respective state-of-the-art techniques while offering stable sensing quality. Further, heat-maps of estimated field signals corresponding to synthetically generated and parsimoniously sensed multi-source parameters are also provided which may aid in source localization Internet-of-Things applications.**

***Index Terms*—Adaptive multi-sensing, energy harvesting-wireless sensor networks (EH-WSNs), network residual energy, cross-correlation, joint sparsity, spatial proximity**

I. Introduction

Internet-of-Things (IoT) applications such as smart environment [2], health-care [3], precision agriculture [4], border surveillance [5], avalanche monitoring, target tracking [6], etc. require simultaneous monitoring of multiple spatio-temporally evolving correlated parameters/signals. One solution to perform this multi-sensing task (i.e., sensing multiple parameters) is to deploy heterogeneous wireless sensor networks (WSNs) for the IoT applications. However, performing this energy-hungry multi-sensing task using battery-constrained wireless nodes severely limits network lifetime. This mandates devise of a smart multi-sensing framework that intelligently optimizes sensing quality of the various to-be-sensed parameters and energy efficiency of the WSN. In addition, the spatio-temporal and cross correlation characteristics of the parameters being monitored can be exploited to impart this intelligence. Though the intelligent multi-sensing prolongs network lifetime, it cannot make the WSNs sustainable due to limited battery capacity of the nodes. To impart network sustainability in energy-intensive multi-sensing applications, such networks use nodes equipped with ambient energy harvester module [7].

A. Related works

Various monolithic sensing approaches (wherein single parameter is sensed) over densely deployed WSNs exist in literature. These approaches use only a few nodes to sense a slowly varying spatio-temporal signal pertaining to an observed process. The conventional ones [8], [9] opted random selection of these fixed number of nodes. Subsequently, several frameworks came out in the literature that select fixed number of sensors to guarantee certain performance measures such as energy efficiency [10], sensing quality [11]–[13], or both [14], [15]. The authors in [16] proposed an integrated data and energy gathering framework, called iDEG, that randomly activates a fixed number of nodes each time for sensing while harvest energy from non-participating nodes. Herein, double sparsity due to spatio-temporal variations of the underlying process is exploited to reconstruct data across entire field using compressed sensing framework. Further, the approach in [17] employed Bayesian framework for field reconstruction across both high and low quality sensors measuring the same process. For sparse heterogeneous sensor selection, maximum allowed uncertainty at the query location is assumed and cross-entropy method is used. However, these works considered an impractical setting of sensing a spatio-temporally varying signal using fixed number of nodes/sensors.

To overcome this limitation, several adaptive sensor selection techniques [18], [19] gained significant research interest. Recently, an adaptive and energy-efficient monolithic sensing framework was proposed in [20] that performs optimized sensor selection by considering the sensing quality, energy efficiency, and process variations. An optimization problem formulation was proposed in [21] that exploits spatial correlation among different sensors, learned from training data, to select a fixed number of sensors. Herein, the training interval is adapted by considering signal variations in the network.

A preliminary version of the work was presented at the IEEE GLOBECOM, Big Island, HI, USA, Dec. 2019 [1].

This work was supported in parts by the Department of Science and Technology, Intl. Bilateral Cooperation Div., grant no. INT/UK/P-153/2017, the Science and Engineering Research Board, grant no. CRG/2019/002293, the Department of Telecommunications, grant no. 4-23/5G test bed/2017-NT for building end to end 5G test-bed, and TCS RSP Fellowship.

The authors are with the Department of Electrical Engineering and Bharti School of Telecommunications, Indian Institute of Technology Delhi, New Delhi 110016, India (e-mail: vini.gupta@ee.iitd.ac.in; swadesd@ee.iitd.ac.in).

The existing infrastructure used for monolithic sensing cannot be directly used for multi-sensing applications. Deployment of dedicated nodes/networks for sensing different parameters is highly resource-inefficient. Further, replication of the large-scale WSNs may significantly increase deployment and maintenance costs. Recent works such as [22]–[25] explored the idea of sharing the network for multi-sensing to overcome the drawbacks of infrastructure replication. In this context, the work in [22] considered a node with multiple sensors that can sense multiple parameters at a given location. A threshold-based hierarchical approach was employed in [24] for data reduction to realize a sustainable heterogeneous sensor system. Likewise, adaptive hierarchical data acquisition models based on context-aware sensing of dependent parameters are proposed for landslide monitoring [25]. Recently, in order to realize the smart environment application of IoT, an adaptive multi-sensing framework was proposed in [1] for an energy harvesting-WSN (EH-WSN). Herein, the to-be-sensed parameters do not depend on each other.

B. Research gap and motivation

The multi-sensing proposals [22], [23] primarily focus on designing platforms to realize multi-sensing. Sensor selection and field estimation aspects are left out. In the hierarchical and threshold-based sensing strategies [24], [25], decisions for sensing dependent parameters are based on measured signal values corrupted with unknown noise. This associated uncertainty raises question on their reliability. Further, these approaches do not deal with multi-sensor data fusion for field estimation which is critical for a monitoring application. Most of the monolithic [16], [17], [21] and multi-sensing [24], [25] strategies do not consider an important aspect of unequal remaining energy of the nodes during sensor selection. It may result in network coverage outage due to repeated selection of a few nodes' sensors. Moreover, these works do not exploit intra- and inter-node collaboration in sensor selection and signal estimation processes which may significantly help respectively in reducing overall network energy consumption and increasing field monitoring accuracy. Besides, none of the existing works on multi-sensing collectively consider process variations, sensing quality and energy consumption trade-off, and node/network-level collaboration for sensor selection.

To overcome these lacuna, an adaptive and energy-efficient multi-sensing framework is proposed to intelligently sense cross-correlated spatio-temporal parameters/signals in an EH-WSN. It accounts dynamics of the observed signals, jointly optimizes sensing quality and network energy efficiency, and integrates inter-/intra-node collaboration to activate a subset of sensors of the nodes. Further, for sparse multi-sensing with intra-node collaboration, a joint sparse recovery scheme is presented that fuses multi-sensory data for field estimation.

C. Contributions and significance

Contributions and significance of this work are as follows:

1) An adaptive and energy-efficient multi-sensing framework, named as MS, is proposed for heterogeneous WSN. It selects a few sensors of each type mounted on different wireless nodes to sense different correlated slowly-varying parameters. For sensing each parameter, a multi-objective optimization (MOP) problem is solved that trades-off between the parameter's sensing quality and network energy efficiency. This heterogeneous sensors selection process is adapted according to the spatio-temporal dynamics of the observed parameters.
2) To further increase energy efficiency, a network collaboration based multi-sensing strategy, termed as MS-SP, is developed. It utilizes spatial proximity of nodes with same type of active sensors, obtained from the MS strategy, to reduce the number of active sensors. Further, a retraining strategy for MS-SP is also presented.
3) A node-level collaborative multi-sensing, called MS-CC, is proposed, where cross-correlation among parameters observed by its active sensor set (obtained from MS-SP) is exploited to further prune this active sensors set.
4) A multi-sensor data fusion technique integrated with the MS-CC for heterogeneous field recovery is presented. It leverages the spatial and cross-correlation among measurements to derive principal component analysis (PCA)-based Kronecker sparsifying basis. The under-sampled sensors measurements obtained from the MS-CC and the sparsifying basis are then employed in sparse Bayesian learning (SBL) technique to jointly estimate sparse field parameters. This collective usage of the spatial, temporal, and cross-correlations among monitored field parameters has never been explored in the existing literature on sensor selection.
5) The proposed strategies are tested on synthetic as well as real WSN data. For synthetic data, a general procedure of generating correlated spatio-temporal environmental parameters is outlined. Heat-maps of these parameters' estimates are provided for an environmental scenario with multiple sources of different pollutants. Unlike the existing literature, this work integrates energy awareness in the multi-sensing framework. Performance comparison of the proposed multi-sensing schemes with the closest approaches demonstrates that up to $\sim 50\%$ gain in energy efficiency is achieved without sacrificing the sensing quality of the observed parameters.

The proposed multi-sensing strategies have diverse utility, such as in smart environment, smart agriculture, environment monitoring, and hazardous gas monitoring.

D. Organization

EH-WSN system model for multiple parameters acquisition and nodes' operational energy cost are presented in Section II. Section III presents the proposed MS strategies and their complexities. Joint sparse recovery of field parameters is described in Section IV, followed by simulation results and concluding remarks, respectively in Sections V and VI.

II. System model: EH-WSN

First, the notations and conventions used are listed below.

In this work, $\mathbf{A} \in \mathbb{R}^{M\times N}$ and $\mathbf{a} \in \mathbb{R}^{N\times 1}$ represent a real-valued matrix of size $M \times N$ and a real vector of

TABLE I: List of symbols

Notation	Description
N	Total number of static wireless nodes
P	Number of heterogeneous sensors per node
$\mathbf{z}_k^p \in \mathbb{R}^{N\times 1}$	Spatial signal corresponding to p^{th} parameter across N nodes in k^{th} cycle
$\mathcal{A}_k^p$	Set containing nodes with active p^{th} sensor
$M_k^p = \lvert\mathcal{A}_k^p\rvert$	Total number of nodes with active p^{th} sensor
$\widetilde{\mathbf{y}}_k^p \in \mathbb{R}^{M_k^p\times 1}$	Measured p^{th} signal corresponding to nodes $\in \mathcal{A}_k^p$
$\mathbf{A}_k^p \in \mathbb{R}^{M_k^p\times N}$	Sensing matrix for p^{th} parameter
$\mathbf{B}_k^p \in \mathbb{R}^{N\times N}$	Sparsification matrix for p^{th} parameter
$\widetilde{\mathbf{y}}_k \in \mathbb{R}^{M_k\times 1}$	Joint measurement vector $\left(M_k = \sum_{p=1}^{P} M_k^p\right)$
$\mathbf{A}_k \in \mathbb{R}^{M_k\times NP}$	Joint sensing matrix for all the P parameters
$\mathbf{z}_k \in \mathbb{R}^{NP\times 1}$	Joint field signals' vector
$E_{op_k}(n)$ (J)	Energy consumed in operations of node n
E_{s_k} (J)	Sensing energy consumed by active sensors of a node
$E_{rem_k}(n)$ (J)	Remaining energy of n^{th} node in k^{th} cycle
E_{h_k} (J)	Solar energy harvested by a node in k^{th} cycle
$[\alpha, \beta]$	Lower and upper limits of BCRB
$M_{k+1\lvert k}^p$	Number of nodes predicted to have active p^{th} sensor in $(k+1)^{th}$ cycle
$\mathcal{I}_k^p$	Set containing nodes with active p^{th} sensors across which the signal is below their detection limit in k^{th} cycle
$\mathcal{I}_{k+1\lvert k}^p$	Predicted set containing nodes across which the p^{th} signal may remain below p^{th} sensors detection limit in $(k+1)^{th}$ cycle

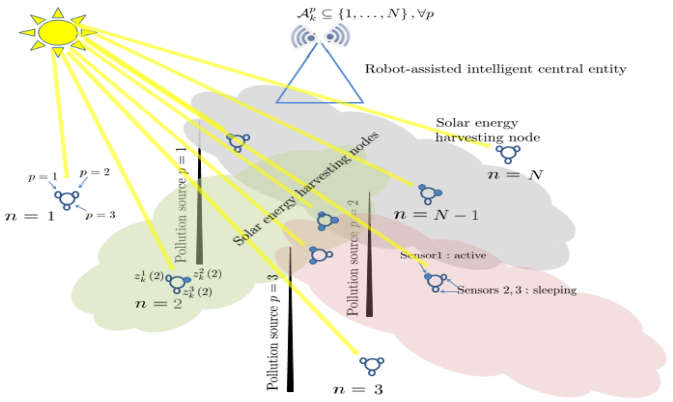

Fig. 1: Multi-sensing in pollution monitoring EH-WSN.

size $N \times 1$ respectively. $\mathbf{I}_N$ represents an $N \times N$ identity matrix. $\mathbf{A}(m,n)$, $A(m,:)$, and $\mathrm{Tr}\{\mathbf{A}\}$ respectively denote the $(m,n)^{th}$ element, m^{th} row, and trace of $\mathbf{A}$. $a(m)$ and $\|\mathbf{a}\|$ denote the m^{th} element and the standard l_2-norm of $\mathbf{a}$ of vector $\mathbf{a}$ respectively. Throughout the paper, superscript p and subscript k refer to the scalar/vector/matrix argument corresponding to p^{th} parameter in k^{th} measurement cycle respectively. The operators $(.)^T$, $\mathrm{diag}(\cdot)$, $|.|$, and $\bigcup$ denote the transpose of the vector/matrix, the standard diagonalization operation on a vector, the cardinality, and the set union operation respectively. The main symbols used in this paper are listed in Table I.

A. Multi-parameter acquisition

An EH-WSN is considered containing N static wireless nodes, each mounted with P heterogeneous sensors to monitor P correlated slowly-varying parameters (such as, CO, SO_2, NO_2, etc., for pollution monitoring application in a solar energy harvesting WSN, as shown in Fig. 1). Each node has solar energy harvesting capability. Different types of sensors have different detection limit. Let the signal corresponding to p^{th} parameter across N nodes in k^{th} measurement cycle be denoted by spatial signal vector $\mathbf{z}_k^p = [z_k^p(1), \cdots, z_k^p(N)]^T \in \mathbb{R}^{N\times 1}$. For each p^{th} parameter, central entity (fusion center (FC)) runs the MOP problem in parallel (discussed in Section III) and selects p^{th} sensor of $M_k^p (\leq N)$ number of nodes for activation during the k^{th} cycle. The corresponding active sets are represented by $\mathcal{A}_k^p \subseteq \{1, \cdots, N\}$ and $|\mathcal{A}_k^p| = M_k^p, \forall p$. The active/sleep status of the sensors is conveyed to the nodes. Let sensing matrix $\mathbf{A}_k^p \in \mathbb{R}^{M_k^p\times N}$ captures the sensing status (active/sleep) of p^{th} sensor of all the nodes. Each row corresponds to p^{th} active sensor of a distinct node out of total M_k^p nodes. If m^{th} row represents i^{th} node's p^{th} active sensor, then the row $A_k^p(m,:)$ is given by,

$$\mathbf{A}_k^p(m,n) = \begin{cases} 1 \text{ (active)} & , n = i \text{ s.t. } i \in \mathcal{A}_k^p \\ 0 \text{ (sleep)} & , n \in \{1,\ldots,N\}\backslash\{i\} \end{cases}.$$

Let the measurement vector $\widetilde{\mathbf{y}}_k^p \in \mathbb{R}^{M_k^p\times 1}$ contains the p^{th} parameter signal sensed by the sensors of nodes $\in \mathcal{A}_k^p$. Thus, for acquiring the p^{th} parameter, $\forall 1 \leq p \leq P$, the system model is given by,

$$\widetilde{\mathbf{y}}_k^p = \mathbf{A}_k^p \mathbf{z}_k^p + \mathbf{n}_k^p, \tag{1}$$

where $\mathbf{n}_k^p \in \mathbb{R}^{M_k^p\times 1}$ denotes white Gaussian noise vector with independent and identically distributed components having zero mean and variance σ^2. Thereafter, a mobile robot/data collector collects active sensors measurements by moving to the nodes and sends them to the FC. The FC then estimates the signal vectors $\mathbf{z}_k^p, \forall p$, separately/jointly and runs sensor selection strategy to broadcast sensing schedule for next measurement cycle. The selected sensors of nodes then sense the respective signals and their measurements are collected by the mobile robot so as to transmit them to the FC. The mobile robot does so in each measurement cycle.

Due to the inherent spatial correlation, a sparse representation of the system model can be derived using the PCA transformation [26],

$$\mathbf{y}_k^p = \mathbf{A}_k^p \mathbf{B}_k^p \mathbf{x}_k^p + \mathbf{n}_k^p, \forall p, \tag{2}$$

where $\mathbf{B}_k^p \in \mathbb{R}^{N\times N}$ is sparsification matrix for the p^{th} parameter signal $\mathbf{z}_k^p$, $\mathbf{x}_k^p \in \mathbb{R}^{N\times 1}$ is corresponding sparse vector, and $\mathbf{y}_k^p \in \mathbb{R}^{M_k^p\times 1}$ is equivalent measurement vector. Before start of first sensing operation, training sets $(\mathcal{T}^p, \forall p)$ containing a few past instances (K_{tr}) of spatial signal $\mathbf{z}_{(\cdot)}^p$ are used to compute $\mathbf{B}_k^p, \forall p$. Later, these sets are updated by including current cycle's estimate of the signal $\mathbf{z}_k^p$. For details on the PCA transformation, please refer work [20].

Note that the mobile robot-based sensed data collection significantly saves transmission energy required by the nodes to send the data to the FC. However, this consideration increases data delivery time (delay), and thus it works well for delay-tolerant applications such as traffic surveillance [27], transmission line monitoring [28], etc. Other delay-tolerant

telemetry applications include animal habitat monitoring and border surveillance [29]. The associated delay can be decreased by using multiple robots to collect data. Further, note that the mobile robot is used only in nodes-to-FC transmission path and not in FC-to-nodes transmission path. In the latter path, the FC directly informs the nodes about respective active sensors by broadcasting the sensing schedule. Thus, the nodes are not completely disconnected from the FC. This process of sensor node activation avoids the robot-induced delay and ensures timely activation and sensing by the sensors compared to the scenario, where the robot is used in the FC-to-nodes transmission path as well.

For real-time (delay-constrained) applications, such as hazardous gas monitoring and health monitoring, the nodes in the considered system model can directly transmit sensed data to the FC as suggested in the survey [30]. This would decrease delay encountered due to inclusion of the mobile robot, however at the cost of nodes' increased energy consumption for data transmission.

It is important to note here that, the channel impairments, such as shadowing and fading, are not taken into account in the current work for two key reasons: (i) The application is considered delay-tolerant and the associated communication infrastructure is suited to it. Any packet loss due to channel variability can be mitigated through channel-aware re-transmission strategies. (ii) Since communication distance from the mobile robot to the individual field nodes is short and nearly the same, the wireless channel related uncertainty and the associated energy overhead in transmitting sensed data are considered negligible and nearly the same for all field nodes. Thus, accounting for the channel gain in the formulation is expected to bring no additional insight, though the network lifetime results may be affected.

B. Wireless node's remaining energy calculation

A wireless node spends energy in sensing, transmission/reception, and data logging. This energy information is vital for multi-sensing problem that aims to improve network efficiency and reduces network energy outage. Often ignored in the literature, this information is integrated in the current work.

Energy consumed in various operations of a node n in measurement cycle $k\,(E_{op_k}(n))$ is given by,

$$E_{op_k}(n) = E_{s_k}(n) + E_{CPU_k} + E_{memory_k} + E_{radio_k}, \quad (3)$$

where $E_{s_k}(n)$ equals total energy consumed by active sensors of the node n (i.e. $E_{s_k}(n) = \sum_{p=1}^{P} E_s^p \times \mathbf{1}(n \in \mathcal{A}_k^p)$ with $\mathbf{1}(\cdot)$ being standard indicator function and E_s^p denotes sensing energy of p^{th} sensor), E_{CPU_k}, E_{memory_k}, and E_{radio_k} respectively represent energy consumed in central processing unit (CPU), memory, and radio operations. For sensing and transmitting the sensed data to the data collector, the sensors and other components of the considered mote (i.e. wireless node) operates in different modes to sequentially perform sensing, data logging, 2-way handshake with the data collector (receive hello, transmit acknowledge), and transmit data to it [31] as shown in Table II.

TABLE II: Different operation modes of mote's components

Operation	Sensor	CPU	Memory	Radio
Sensing	Active	Sleep	Off	Off
Data Logging	Sleep	Active	Write	Off
Receive hello	Sleep	Active	Off	Transmit
Transmit acknowledge	Sleep	Active	Off	Receive
Transmit data	Sleep	Active	Read	Transmit

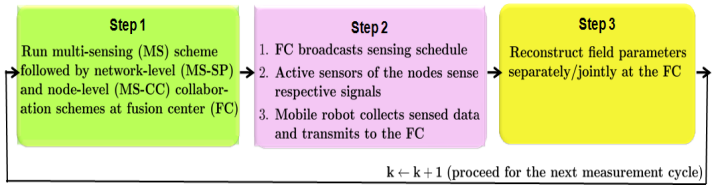

Fig. 2: Multi-sensing framework.

The energy consumed in active/sleep modes of sensors are obtained from their data-sheets [31]. It depends on sensor type used and its measurement time.

After transmission of sensed data to the data collector, remaining energy of each node is updated in every cycle as follows:

$$E_{rem_k}(n) = E_{rem_{k-1}}(n) - E_{op_k}(n) + E_{h_k}, \quad (4)$$

where $E_{rem_k}(n)$ is the remaining energy of the n^{th} node after k^{th} cycle and E_{h_k} represents solar energy harvested by the harvester mounted on the node. The energy harvesting profile is considered similar to [1] with hourly solar irradiance $D_h = [0.039, 0.124, 0.209, \cdots, 0]$ for $h = [8:30\text{am}, 9:30\text{am}, 10:30\text{am}, \cdots, 7:30\text{am}]$ [32] in the simulations. It may be noted that, the multi-sensing strategies proposed in the subsequent section are applicable with ambient energy harvesting capability of the nodes; in this study solar energy harvesting is considered.

Further, it is assumed that the remaining energy information of the nodes with active sensors is integrated with the measured signal of these nodes and sent to the FC via the robot. For the nodes with all the sleeping sensors, it is assumed that the FC has full knowledge of the harvested energy (E_{h_k}) and energies consumed by the sensors, CPU, memory, and radio in sleeping mode during various operations of the nodes (i.e. $E_{op_k}(\cdot)$) mentioned in Table II. Using this knowledge, it updates remaining energy of nodes with all sleeping sensors.

III. Multi-sensing Strategies

The proposed multi-sensing strategies that exploit spatial, temporal, and cross-correlation are outlined in this section. The schematic of the framework is shown in Fig. 2. In step 1, the FC executes multi-sensing (MS) strategy wherein P multi-objective optimization problems are run in parallel, one each for selection of a type of sensor. This is followed by execution of the network-level (MS-SP) and node-level (MS-CC) schemes at the FC. In step 2, the FC broadcasts the sensing schedule. Selected sensors of the nodes sense the respective signals. Thereafter, a mobile robot collects the sensed signals from the nodes with active sensors and transmits to the FC. In step 3, the FC reconstructs field parameters.

Thereafter, the same process (step 1 $\rightarrow$ step 2 $\rightarrow$ step 3) follows in the next measurement cycle.

A. Adaptive multi-sensing (MS)

During each measurement cycle, for each parameter, the FC runs adaptive sensor selection and signal estimation tasks in parallel. For the latter task, the SBL framework [33] is employed which uses the vector $\mathbf{y}_k^p$ and matrices $\mathbf{A}_k^p, \mathbf{B}_k^p$ of (2) to obtain an estimate of the p^{th} sparse signal $\widehat{\mathbf{x}}_k^p \in \mathbb{R}^{N\times 1}$. From $\widehat{\mathbf{x}}_k^p$, estimate of the parameter signal $\widehat{\mathbf{z}}_k^p$ is obtained using the PCA transformation and $\mathbf{B}_k^p$ [20]. Further, an important and often-ignored heterogeneous sensing constraint is integrated with the recovery and sensing tasks (discussed below): the active p^{th} sensor of the nodes $\in \mathcal{A}_k^p$ do not participate in the recovery task if the signal $z_k^p(\cdot)$ across them is below their detection limit ρ^p because the corresponding measured signal $y_k^p(\cdot) = 0$. Such node(s) constitute a set $\mathcal{I}_k^p\,(\subseteq \mathcal{A}_k^p$ or $\emptyset)$.

For sensing P parameters in each $(k+1)^{th}$ cycle, active sensors of the nodes are obtained by solving P multi-objective optimization problems (MOPs) (5) in parallel using scalarization technique [1]:

$$\underset{\widetilde{\mathbf{A}}_{k+1}^p(n,n)\ \forall n}{\text{minimize}} \ \left(1-\lambda_{k+1}^p\right)\text{Tr}\left\{\left(\frac{1}{\sigma^2}\left(\mathbf{B}_{k+1}^p\right)^T\widetilde{\mathbf{A}}_{k+1}^p\left(\mathbf{B}_{k+1}^p\right)+\left(\mathbf{\Gamma}_{k+1}^p\right)^{-1}\right)^{-1}\right\} + \lambda_{k+1}^p\left(\sum_{n=1}^{N}\frac{1}{E_{rem_k}(n)}\widetilde{\mathbf{A}}_{k+1}^p(n,n)\right)$$

$$\text{subject to} \quad \widetilde{\mathbf{A}}_{k+1}^p(n,n)\in\{0,1\},\ n=1,\ldots,N \tag{5a}$$

$$\widetilde{\mathbf{A}}_{k+1}^p(n,n)=0,\ n\in\{i\mid E_{rem_k}(i)=0\} \tag{5b}$$

$$\sum_{j\in\mathcal{R}_r}\widetilde{\mathbf{A}}_{k+1}^p(j,j)\geq 1,\ r=1,\ldots,R \tag{5c}$$

$$\widetilde{\mathbf{A}}_{k+1}^p(n,n)=0,\ n\in\mathcal{I}_{k+1|k}^p. \tag{5d}$$

$\text{Tr}\left\{\left(\frac{1}{\sigma^2}\left(\mathbf{B}_{k+1}^p\right)^T\widetilde{\mathbf{A}}_{k+1}^p\mathbf{B}_{k+1}^p+\left(\mathbf{\Gamma}_{k+1}^p\right)^{-1}\right)^{-1}\right\}$ represents Bayesian Cramér-Rao bound (BCRB) which characterizes unknown mean squared error [1], [20]. The entity $\widetilde{\mathbf{A}}_{k+1}^p = \left(\mathbf{A}_{k+1}^p\right)^T\mathbf{A}_{k+1}^p \in \mathbb{R}^{N\times N}$ is a binary diagonal matrix with $\widetilde{\mathbf{A}}_{k+1}^p(n,n) = 1/0$ denoting active/sleep status of the n^{th} node's p^{th} sensor. The weighted sensor selection function $\sum_{n=1}^{N}\frac{1}{E_{rem_k}(n)}\widetilde{\mathbf{A}}_{k+1}^p(n,n)$ promotes selection of the p^{th} sensor of the nodes with higher remaining energy left after k^{th} cycle, i.e. $E_{rem_k}(\cdot)$. Thus, the MOP (5) jointly optimizes the sensing quality and network energy efficiency. Constraint (5a) captures active(1)/sleep(0) state of the p^{th} sensor of n^{th} node. Constraint (5b) accounts the fact that sensors of the node(s) with zero remaining energy cannot participate. For better monitoring of the field parameter, coverage constraint (5c) activates p^{th} sensor of at least one node from each coverage region $\mathcal{R}_r, \forall\ 1\leq r\leq R$. The WSN field is assumed to be divided into R fixed non-overlapping regions. Let a predicted set $\mathcal{I}_{k+1|k}^p$ comprises nodes across which the signal $z_{k+1}^p(\cdot)$ may remain below the p^{th} sensor's detection limit. Its construction is discussed below along with the adaptation mechanism. Detection limit constraint (5d) prevents selection of p^{th} sensor of nodes $n\in\mathcal{I}_{k+1|k}^p$. The scalarization technique converts an MOP into a single objective optimization problem by associating scalar weights with each objective function. Usually, the scalar weights $\in[0,1]$ and their sum equals 1. Here, multiple objective functions, namely BCRB and sensor selection, are converted to single objective function in (5) using the weights $\left(1-\lambda_{k+1}^p\right)$ and λ_{k+1}^p. The MOP (5) is non-convex in nature due to the binary constraint (5a) and hard to solve. Applying exhaustive search over $\binom{N}{m}, \forall\ 1\leq m\leq N$, combinations to solve it is impractical for the considered dense WSN deployment settings. Thus, the constraint (5a) is relaxed to box constraint: $\widetilde{\mathbf{A}}_{k+1}^p(n,n)\in[0,1], \forall n$ [20]. Due to this, the relaxed scalarized MOP, given by (6), becomes a convex problem.

$$\underset{\widetilde{\mathbf{A}}_{k+1}^p(n,n)\ \forall n}{\text{minimize}} \ \left(1-\lambda_{k+1}^p\right)\text{Tr}\left\{\left(\frac{1}{\sigma^2}\left(\mathbf{B}_{k+1}^p\right)^T\widetilde{\mathbf{A}}_{k+1}^p\left(\mathbf{B}_{k+1}^p\right)+\left(\mathbf{\Gamma}_{k+1}^p\right)^{-1}\right)^{-1}\right\} + \lambda_{k+1}^p\left(\sum_{n=1}^{N}\frac{1}{E_{rem_k}(n)}\widetilde{\mathbf{A}}_{k+1}^p(n,n)\right)$$

$$\text{subject to} \quad \widetilde{\mathbf{A}}_{k+1}^p(n,n)\in[0,1],\ n=1,\ldots,N \tag{6a}$$

$$\widetilde{\mathbf{A}}_{k+1}^p(n,n)=0,\ n\in\{i\mid E_{rem_k}(i)=0\} \tag{6b}$$

$$\sum_{j\in\mathcal{R}_r}\widetilde{\mathbf{A}}_{k+1}^p(j,j)\geq 1,\ r=1,\ldots,R \tag{6c}$$

$$\widetilde{\mathbf{A}}_{k+1}^p(n,n)=0,\ n\in\mathcal{I}_{k+1|k}^p. \tag{6d}$$

Given scalar variable λ_{k+1}^p in each measurement cycle, the relaxed scalarized MOP (6) is solved using CVX [34]. Due to simultaneous optimization of two contradicting functions and box constraint $\widetilde{\mathbf{A}}_{k+1}^p(n,n)\in[0,1]$, the optimized values of $\widetilde{\mathbf{A}}_{k+1}^p(n,n), \forall n$ are either close to 1 or close to 0 (observed in simulations as well). Thus, to obtain the entity M_{k+1}^p, adding $\widetilde{\mathbf{A}}_{k+1}^p(n,n)$ corresponding to all N nodes followed by rounding the sum to nearest integer is intuitive, as shown in (7). The unknown entity $\mathcal{A}_{k+1}^p$ is obtained as given in (8).

$$M_{k+1}^p = \text{round}\left(\sum_{n=1}^{N}\widetilde{\mathbf{A}}_{k+1}^p(n,n)\right), \tag{7}$$

$$\mathcal{A}_{k+1}^p = \text{Row indices of } M_{k+1}^p \text{ largest elements of set: } \left\{\widetilde{\mathbf{A}}_{k+1}^p(n,n)\middle|\widetilde{\mathbf{A}}_{k+1}^p(n,n)\geq\widetilde{\mathbf{A}}_{k+1}^p(m,m)\,\forall n,m\right\} \tag{8}$$

Note that, after rounding, the result of the MOP (6) can be interpreted as $\widetilde{\mathbf{A}}_{k+1}^p(n,n)=1$ for all the nodes n with active p^{th} sensor, i.e., $n\in\mathcal{A}_{k+1}^p$ and $\widetilde{\mathbf{A}}_{k+1}^p(m,m)=0$ for the nodes m with sleeping p^{th} sensor, i.e., $m\notin\mathcal{A}_{k+1}^p$. Thus, the result is feasible to the original problem (5) which assigns binary values $0/1$ to the variables $\widetilde{\mathbf{A}}_{k+1}^p(n,n), \forall n$. Further, it can be observed that $\widetilde{\mathbf{A}}_{k+1}^p\left(=\left(\mathbf{A}_{k+1}^p\right)^T\mathbf{A}_{k+1}^p\in\mathbb{R}^{N\times N}\right)$ is a positive semi-definite matrix (binary diagonal matrix) which is ensured by the solution of the relaxed MOP (6) as well.

Adaptation process: The scalar weight λ_{k+1}^p is obtained by employing modified binary search (MBS) proposed in [20] with an additional input $\mathcal{I}_{k+1|k}^p$. The MBS searches λ_{k+1}^p in space $[0,1]$ to minimize the MOP (6) until either $(\lambda_{k+1}^p)_U-(\lambda_{k+1}^p)_L<\Delta$ or $\sum_{n=1}^{N}\widetilde{\mathbf{A}}_{k+1}^p(n,n)==M_{k+1|k}^p$ is satisfied; Δ being a small positive real number. Input $M_{k+1|k}^p$ (calculated in previous cycle k) to the MBS algorithm denotes the number of nodes predicted to have p^{th} active sensor in

$(k+1)^{th}$ cycle. It is adapted on the basis of estimated p^{th} parameter's variation in the previous cycle k ($\widehat{\delta}_k^p$) and updated remaining energy of the nodes such that the BCRB remains within a desired application-specific range $[\alpha, \beta]$. Intuitively, higher parameter variation demands more active sensors. Thus, if $\widehat{\delta}_k^p > \delta_{th}^p$, then $M_{k+1|k}^p \leftarrow M_k^p + 1$, where $\widehat{\delta}_k^p = \frac{\left\|\widehat{\mathbf{z}}_k^p - \widehat{\mathbf{z}}_{k-1}^p\right\|}{\sqrt{N}}$ and δ_{th}^p is a suitably chosen threshold. Else, construct a pruned active set $\mathcal{A}_{k|M_k^p-i}^p$ (i.e. $\mathcal{A}_k^p \setminus \{i \text{ nodes}\}$) by decreasing M_k^p in unit steps ($M_{k+1|k}^p \leftarrow M_k^p - i, \forall i = 1, \cdots, M_k^p - R$) and compute a heuristic $\widehat{\epsilon}_k^p = \left\|\widehat{\mathbf{x}}_k^p - \widehat{\mathbf{x}}_{k|M_k^p-i}^p\right\|$. This heuristic determines the extent up to which M_k^p can be decreased in the next $(k+1)^{th}$ cycle such that the estimates $\widehat{\mathbf{x}}_k^p$ and $\widehat{\mathbf{x}}_{k|M_k^p-i}^p$ are nearly same. If $\widehat{\epsilon}_k^p \leq \epsilon_{th}^p$ and corresponding $\text{BCRB}_{k|M_k^p-i}^p \in [\alpha, \beta]$, further decrease M_k^p until either $\text{BCRB}_{k|M_k^p-i}^p \notin [\alpha, \beta]$ or $M_k^p - i < R$. Next, the predicted entities $\mathcal{I}_{k+1|k}^p$ and $M_{k+1|k}^p$ are updated (in previous cycle k) based on the set $\mathcal{I}_k^p$ and slow variations of the parameter as,

$$\left.\begin{array}{l}\mathcal{I}_{k+1|k}^p \leftarrow \emptyset, \text{ if } \mathcal{I}_k^p = \emptyset \\ \mathcal{I}_{k+1|k}^p \leftarrow \mathcal{I}_k^p, \text{if } \mathcal{I}_k^p \neq \emptyset, \widehat{\delta}_k^p \leq \delta_{th}^p \\ \mathcal{I}_{k+1|k}^p \leftarrow \emptyset, \text{if } \mathcal{I}_k^p \neq \emptyset, \widehat{\delta}_k^p > \delta_{th}^p\end{array}\right\}, M_{k+1|k}^p = \min\{M_k^p, N - |\mathcal{I}_k^p|\}. \tag{9}$$

From output of the MBS, if $\sum_{n=1}^N \widetilde{\mathbf{A}}_{k+1}^p(n,n) = M_{k+1|k}^p$ and corresponding $\text{BCRB}_{k+1} \in [\alpha, \beta]$, continue with sensing task of the next measurement cycle. Otherwise, if $\text{BCRB}_{k+1} < \alpha$ (or $> \beta$), then update $M_{k+1|k}^p \leftarrow \max\left\{M_{k+1|k}^p - 1, R\right\}$ $\left(\text{or } \min\left\{M_{k+1|k}^p + 1, N\right\}\right)$.

A step-wise schematic of the proposed adaptive multi-sensing framework is outlined in Algorithm 1 which the FC runs in parallel for each parameter p.

B. Network-level collaboration-based multi-sensing (MS-SP)

This strategy uses inter-node (or network-level) collaboration to further reduce size of the active sets ($\mathcal{A}_k^p, \forall p$) obtained from the MS strategy by turning off the nodes $\left(\in \mathcal{A}_k^{(\cdot)}\right)$ with only one active sensor. To do so, **s**patial **p**roximity among nodes with same type of active sensors is exploited, hence, the strategy is termed as **MS-SP**. The logic developed is as follows: nodes with only one active sensor (say type p), constitute a set $\mathcal{A}1_k^p$, are turned OFF if there exists more than one nearest neighbor node with more than one active sensor including type p. The process of turning off sensors saves energies ($E_{s_k}, E_{CPU_k}, E_{radio_k}$, and E_{memory_k}). Step-wise flow is given below-

1) Construct the set $\mathcal{A}1_k^p$ as $\mathcal{A}1_k^p = \{n | (n \in \mathcal{A}_k^p) \cap (n \notin \mathcal{A}_k^q), \forall q \neq p, 1 \leq n \leq N\}$.
2) For each $n \in \mathcal{A}1_k^p$, create a set of its nearest neighbor nodes with respect to the p^{th} parameter signal during cycle k, denoted by $\mathcal{N}_k^p(n)$. It is constructed as follows: if with respect to node n, difference between the p^{th} parameter signal across nodes n, m is less than heuristically chosen values, then the node m is designated as nearest neighbor of the node n with respect to the p^{th} signal. Mathematically, $\mathcal{N}_k^p(n) = \left\{m | \widehat{\Delta z}_{nk-1}^p(m) < \zeta \times \max\left(\widehat{\boldsymbol{\Delta z}_{\boldsymbol{n}k-1}}^p\right), 1 \leq m \leq N\right\} \setminus n$, with the difference signal $\widehat{\Delta z}_{nk-1}^p(m) = |\widehat{z}_{k-1}^p(m) - \widehat{z}_{k-1}^p(n)| \in \mathbb{R}^{N \times 1}, 1 \leq m \leq N$. Note that $\mathcal{N}_k^p(n)$ changes with different nodes (n), parameter signal (p), and measurement cycle (k).
3) If $|\mathcal{N}_k^p(n) \in \mathcal{A}_k^p \setminus \mathcal{A}1_k^p| > 1, \forall n \in \mathcal{A}1_k^p$, update the p^{th} active set as $\mathcal{A}_k^p \leftarrow \mathcal{A}_k^p \setminus n$ and $M_k^p = |\mathcal{A}_k^p|$.

Retraining: For each parameter, the sparse recovery process

Algorithm 1 Adaptive multi-sensing framework

Input: $\mathcal{T}^p = \{\mathbf{z}_{-K_{tr}+1}^p, \ldots, \mathbf{z}_{-1}^p, \mathbf{z}_0^p\}, \mathcal{R}_r \forall r, \alpha, \beta, \delta_{th}^p, \epsilon_{th}^p, \rho^p$.
Initialization: $\mathbf{E}_{rem_1}, \lambda_1^p, k=1, exitflag^p = 0, \mathcal{I}_1^p = \emptyset$.
while $exitflag^p == 0$ **do**
  if $k = 1$ **then**
    -Calculate $\mathbf{B}_k^p$ using PCA scheme [20].
    -Solve (5) to get $M_k^p, \mathcal{A}_k^p$; obtain $\mathbf{A}_k^p$ (Sec. II-A).
  end if
  Broadcast sensing schedule $\mathcal{A}_k^p$, collect $\mathbf{y}_k^p$.
  Find $\mathcal{I}_k^p$. Use $\{y_k^p(n), n \in \mathcal{A}_k^p \setminus \mathcal{I}_k^p\}$, SBL [33] to get $\widehat{\mathbf{x}}_k^p$.
  Obtain $\widehat{\mathbf{z}}_k^p$ using $\widehat{\mathbf{x}}_k^p$ and PCA transformation [20].
  if $\sum_{n=1}^N E_{rem_k}(n) > 0$ **then** (`Prediction step`)
    Initialize $M_{k+1|k}^p \leftarrow M_k^p$.
    Compute $\widehat{\delta}_k^p$ (Sec. III-A).
    if $\widehat{\delta}_k^p > \delta_{th}^p$ **then**
      $M_{k+1|k}^p \leftarrow M_k^p + 1$.
    else
      for $i = 1, \ldots, M_k^p - R$ **do**
        Construct $\mathcal{A}_{k|M_k^p-i}^p$ (Sec. III-A), $\mathbf{A}_{k|M_k^p-i}^p$.
        Obtain $\widehat{\mathbf{x}}_{k|M_k^p-i}^p$using SBL.
        Compute $\text{BCRB}_{k|M_k^p-i}^p$, $\widehat{\epsilon}_k^p$ (Sec. III-A).
        if $\widehat{\epsilon}_k^p \leq \epsilon_{th}^p$ and $\text{BCRB}_{k|M_k^p-i}^p \in [\alpha, \beta]$ **then**
          $M_{k+1|k}^p \leftarrow M_k^p - i$.
        else if $\text{BCRB}_{k|M_k^p-i}^p \notin [\alpha, \beta]$ **then** $break$.
        end if
      end for
    end if
    Update: $\mathbf{B}_{k+1}^p$(use $\widehat{\mathbf{z}}_k^p$ in PCA). (`Update step`)
    Obtain $\mathcal{I}_{k+1|k}^p$ using (9).
    do
      Call Alg. Modified Binary Search [20] with inputs $\mathbf{E}_{rem_k}, \mathbf{B}_{k+1}^p, M_{k+1|k}^p, \mathcal{I}_{k+1|k}^p, \forall p$.
      if $\sum_{n=1}^N \widetilde{\mathbf{A}}_{k+1}^p(n,n) == M_{k+1|k}^p$ **then**
        Obtain $\mathcal{A}_{k+1}^p, \mathbf{A}_{k+1}^p$.
        Calc. BCRB_{k+1}^p (Sec. III-A).
        if $\text{BCRB}_{k+1}^p < \alpha$ **then**
          $M_{k+1|k}^p \leftarrow \max\left\{M_{k+1|k}^p - 1, R\right\}$.
        else if $\text{BCRB}_{k+1}^p > \beta$ **then**
          $M_{k+1|k}^p \leftarrow \min\left\{M_{k+1|k}^p + 1, N\right\}$.
        end if
      else
        $exitflag^p \leftarrow 1$, $break$.
      end if
    while $\text{BCRB}_{k+1}^p \notin [\alpha, \beta]$.
    Update: $M_{k+1}^p \leftarrow M_{k+1|k}^p$.
  else
    $exitflag^p \leftarrow 1$.
  end if
  Update: $k \leftarrow k + 1$.
end while
Output: $K = k$.

is based on the sparsification matrix $\mathbf{B}_k^p$ which is estimated using a few past instances of estimated signal $\widehat{\mathbf{z}}_{(\cdot)}^p$ or $\widehat{\mathbf{x}}_{(\cdot)}^p$. Due to accumulation of the estimation error, the recovery process may become erroneous as the measurement cycles progress. It may produce non-sparse estimate $\widehat{\mathbf{x}}_k^p$ of the unknown sparse signal $\mathbf{x}_k^p$. To prevent this, a logic to detect need for retraining in the next measurement cycle is proposed which is based on current reconstructed signal vector $\widehat{\mathbf{x}}_k^p$ as the true signal vector $\mathbf{x}_k^p$ is unknown. It is integrated with the MS-SP strategy and termed as **MS-SP retrain**. The key idea is to approximately find and compare the number of non-sparse components $\widehat{NC}_k^p$ in the reconstructed signal $\widehat{\mathbf{x}}_k^p$ against a suitable threshold value NC_{th}^p. If $\widehat{NC}_k^p > NC_{th}^p$, retrain the network in the next $(k+1)^{th}$ cycle. A component $\widehat{x}_k^p(\cdot)$ is considered as non-sparse if it constitutes more than 0.1% of total energy of parameter signal vector $\widehat{\mathbf{x}}_k^p$, i.e., $\frac{\left(\widehat{x}_k^p(\cdot)\right)^2}{\sum_{n=1}^{N}\left(\widehat{x}_k^p(n)\right)^2} > \frac{0.1}{100}$. The 0.1% energy criteria ensures that no non-sparse component of $\widehat{\mathbf{x}}_r^{(k)}$ is wrongly considered as sparse. From the instances of training/retraining signal, the knowledge of NC_{th}^p can be roughly obtained.

C. Node-level collaboration-based multi-sensing (MS-CC)

This strategy exploits intra-node (or node-level) collaboration to further prune active sets obtained from the MS-SP strategy. For each node, active set $\mathcal{P}_k^n$ of sensors is derived from the MS-SP based $\mathcal{A}_k^p, \forall p$ and cross-correlation among signals across its active sensors is computed. Intuitively, highly cross-correlated signals across different sensors of a node can be parsimoniously sensed. Thus, a sensor of n^{th} node $(\in \mathcal{P}_k^n)$ which has high correlation with maximum number of other active sensors of that node $(\in \mathcal{P}_k^n)$, referred as primary sensor, remains ON. The remaining sensors $(\in \mathcal{P}_k^n)$ with which this primary sensor has high (low) correlation are turned OFF (ON). The flow of strategy is as follows:

1) For every node n, compute $\mathcal{P}_k^n = \{p | n \in \mathcal{A}_k^p, 1 \le p \le P\}$. Let number of active sensors of a node be represented by $S_k^n = |\mathcal{P}_k^n|$.
2) Calculate cross-correlation matrix of sensors $\in \mathcal{P}_k^n$, denoted by $\mathbf{C} \in \mathbb{R}^{S_k^n \times S_k^n}$. Pearson correlation coefficient among previously estimated parameter signal $\widehat{z}_{(\cdot)}^p(n)$ is used to compute the matrix $\mathbf{C}$. Do so for each node n.
3) Find correlation degree vector $\mathbf{c} \in \mathbb{R}^{1 \times S_k^n}$ as follows: $c(p) = \sum_{q=1}^{S_k^n} \mathbf{1}(\mathbf{C}(q,p) \ge \eta), 1 \le p \le S_k^n$, where the indicator function $\mathbf{1}(\mathbf{C}(q,p) \ge \eta) = \begin{cases} 1, & \text{if } \mathbf{C}(q,p) \ge \eta \\ 0, & \text{if } \mathbf{C}(q,p) < \eta \end{cases}$. Obtain primary sensor u of node n such that $c(u) = \max_{\forall q}(c(q))$. Repeat this for all the nodes.
4) Update $\mathcal{P}_k^n \leftarrow \mathcal{P}_k^n \setminus p$ and $\mathcal{A}_k^p \leftarrow \mathcal{A}_k^p \setminus n$ if $\mathbf{C}(u,p) \ge \eta, \forall p \in \mathcal{P}_k^n, p \ne u$. Set $M_k^p = |\mathcal{A}_k^p|$. Similarly update for other nodes.

Note, $\eta = 0.5$ is chosen because the literature on signal statistics identifies correlation value 0.5 as high correlation between two signals [35]. Since, **c**ross-**c**orrelation among sensors is used to further decrease active number of sensors of a node, the strategy is known as **MS-CC**. It saves more energy compared to the MS and MS-SP strategies.

Adaptation in MS-CC is based on updated M_k^p if corresponding $\text{BCRB}_k^p \in [\alpha, \beta]$; otherwise M_k^p obtained from the MS strategy is set as predicted value $M_{k+1|k}^p$.

D. Complexity analysis

Let the complexity of recovery scheme, that is executed at the FC, be denoted by $\mathcal{O}_{Rec}$ in general. The complexity of the adaptive multi-sensing framework for each parameter type p is derived by computing complexities of the prediction and the update steps in one measurement cycle. In the prediction step, the complexities of calculating $\widehat{\delta}_k^p$ and $M_{k+1|k}^p$ are $\mathcal{O}(N)$ and $\mathcal{O}\left((M_k^p)^3\right)$, respectively. The overall complexity of the prediction step is given by $\approx \left(\mathcal{O}(N) + \mathcal{O}\left((M_k^p)^3\right) + \mathcal{O}_{Rec}\right)$. In the update step, the complexity of computing $\mathbf{B}_{k+1}^p$ is $\mathcal{O}(N^2)$. The modified binary search requires $\log_2\left(\frac{\lambda_{U_1} - \lambda_{L_1}}{\Delta}\right)$ iterations with each solving the relaxed MOP (6) using the CVX tool. The CVX runs infeasible primal-dual predictor-corrector interior point algorithm based on HKM search direction with complexity $\approx \mathcal{O}\left(\widetilde{N}\log\left(\frac{1}{\nu}\right)\right)$ [36], where $\widetilde{N}$ denotes the number of variables after converting problem (6) to a standard form by the CVX and ν represents the precision accuracy (10^{-8} by default). $\widetilde{N}$ is a function of N. Thus, complexity of the MOP increases with N. Complexity of the update steps is $\mathcal{O}\left((M_{k+1|k}^p)^3\right)$. In the worst case, the update step will converge in $\left(M_{k+1|k}^p - R + 1\right)$ iterations. Thus its overall complexity is $\approx \left(\mathcal{O}\left((M_{k+1|k}^p)^3\right) + \left(M_{k+1|k}^p - R + 1\right)\log_2\left(\frac{1}{\Delta}\right)\mathcal{O}\left(\widetilde{N}\log\left(\frac{1}{\nu}\right)\right)\right)$. Hence, the combined complexity of the proposed adaptive multi-sensing (MS) framework is $\mathcal{O}_{MS} \approx \left(\mathcal{O}\left(max\left(N, (M_k^p)^3\right)\right) + \mathcal{O}_{Rec} + \mathcal{O}\left((M_{k+1|k}^p)^3\right) + \left(M_{k+1|k}^p - R + 1\right)\log_2\left(\frac{1}{\Delta}\right)\mathcal{O}\left(\widetilde{N}\log\left(\frac{1}{\nu}\right)\right)\right)$. Though the framework runs for P parameters/signals in parallel, the complexity remains $\mathcal{O}_{MS}$. On the similar lines, complexities of the MS-SP and MS-CC parts are $(\mathcal{O}_{MS} + \mathcal{O}(NP))$ and $\left(\mathcal{O}_{MS} + \mathcal{O}\left(NP^2\right)\right)$, respectively. Also, the complexity $\mathcal{O}_{Rec}$ for reconstruction of parameters individually (in MS and MS-SP) and jointly (given in subsequent section for MS-CC) using the SBL are $\mathcal{O}\left((M_k^p)^3\right)$ and $\mathcal{O}\left(\left(\sum_{p=1}^{P} M_k^p\right)^3\right) + \mathcal{O}\left(N^2P^2\right)$, respectively.

IV. Joint Sparse Recovery of Field Parameters

Until now, estimation of different field parameters, using measurements of active sensors obtained from the MS and MS-SP strategies, is carried out separately for each parameter at the FC. However, the separate estimation of each parameter does not exploit cross-correlation among them. For the cross-correlation based MS-CC, an estimation scheme is developed that jointly estimates the correlated spatial parameters. This scheme exploits sparsity due to cross, spatial, and temporal correlation of the field parameters.

For joint recovery of the field parameters, the system model (1) is collated as follows:

$$\widetilde{\mathbf{y}}_k = \mathbf{A}_k \mathbf{z}_k + \mathbf{n}_k, \tag{10}$$

where $\widetilde{\mathbf{y}}_k = \text{vec}\left(\left[\widetilde{\mathbf{y}}_k^1, \cdots, \widetilde{\mathbf{y}}_k^P\right]\right) \in \mathbb{R}^{M_k \times 1}$ with $M_k = \sum_{p=1}^{P} M_k^p$, $\mathbf{A}_k = \text{diag}\left(\mathbf{A}_k^1, \cdots, \mathbf{A}_k^P\right) \in \mathbb{R}^{M_k \times NP}$ is a block-diagonal matrix, the field signal $\mathbf{z}_k = \text{vec}\left(\left[\mathbf{z}_k^1, \cdots, \mathbf{z}_k^P\right]\right) \in \mathbb{R}^{NP \times 1}$, and the noise $\mathbf{n}_k = \text{vec}\left(\left[\mathbf{n}_k^1, \cdots, \mathbf{n}_k^P\right]\right) \in \mathbb{R}^{M_k \times 1}$.

In the existing literature on joint sparse signal representation and recovery, Kronecker product of discrete cosine/Fourier transforms-based sparsification matrices is used [16]. However, these matrices do not sparsify the correlated signals well, while PCA does so, as mentioned in [37]. PCA-based joint sparse signal representation has not been explored earlier. To this end, this work derives joint sparse representation of the system (10) using sparsification matrix which is Kronecker product of PCA-based spatial and cross-correlation bases.

Let the matrix $\mathbf{Z}_k = \left[\mathbf{z}_k^1, \cdots, \mathbf{z}_k^P\right] \in \mathbb{R}^{N \times P}$. Using the PCA transformation [26], sparse representation of $\mathbf{Z}_k$ and $(\mathbf{Z}_k)^T \in \mathbb{R}^{P \times N}$ can be written as,

$$\mathbf{Z}_k = \mathbf{B}_k^{sp} \mathbf{X}_k^{sp} + \overline{\mathbf{Z}_k}, \tag{11}$$

$$(\mathbf{Z}_k)^T = \mathbf{B}_k^{cc} \mathbf{X}_k^{cc} + \overline{(\mathbf{Z}_k)^T}, \tag{12}$$

where $\mathbf{B}_k^{sp} \in \mathbb{R}^{N \times N}, \mathbf{B}_k^{cc} \in \mathbb{R}^{P \times P}$ respectively represent spatial and cross-correlation based sparsification matrices, $\mathbf{X}_k^{sp} \in \mathbb{R}^{N \times P}, \mathbf{X}_k^{cc} \in \mathbb{R}^{P \times N}$ are respective sparse signal matrices, and $\overline{\mathbf{Z}_k} \in \mathbb{R}^{N \times P}, \overline{(\mathbf{Z}_k)^T} \in \mathbb{R}^{P \times N}$ are corresponding mean matrices. Using (11), sparse representation of the field signal $\mathbf{z}_k = \text{vec}(\mathbf{Z}_k)$ is derived as follows:

$$\mathbf{z}_k = \text{vec}\left(\mathbf{B}_k^{sp} \mathbf{X}_k^{sp}\right) + \text{vec}\left(\overline{\mathbf{Z}_k}\right), \tag{13}$$

$$= \text{vec}\left(\mathbf{B}_k^{sp} \mathbf{X}_k^{sp} \left(\mathbf{B}_k^{cc}\right)^{-T} \left(\mathbf{B}_k^{cc}\right)^T\right) + \text{vec}\left(\overline{\mathbf{Z}_k}\right) \tag{14}$$

Let the sparse signal $\mathbf{X}_k = \mathbf{X}_k^{sp} \left(\mathbf{B}_k^{cc}\right)^{-T} \in \mathbb{R}^{N \times P}$, $\mathbf{x}_k = \text{vec}(\mathbf{X}_k)$, and using matrix identity $\text{vec}(\mathbf{PRQ}) = \left((\mathbf{Q})^T \otimes \mathbf{P}\right) \text{vec}(\mathbf{R})$ [38], (14) can be written as,

$$\mathbf{z}_k = \left(\mathbf{B}_k^{cc} \otimes \mathbf{B}_k^{sp}\right) \text{vec}(\mathbf{X}_k) + \text{vec}\left(\overline{\mathbf{Z}_k}\right), \tag{15}$$

$$= \left(\mathbf{B}_k^{cc} \otimes \mathbf{B}_k^{sp}\right) (\mathbf{x}_k) + \text{vec}\left(\overline{\mathbf{Z}_k}\right). \tag{16}$$

Substituting (16) in (10), joint sparse representation of the system is given by,

$$\mathbf{y}_k = \mathbf{A}_k \mathbf{B}_k \mathbf{x}_k + \mathbf{n}_k, \tag{17}$$

with $\mathbf{y}_k = \widetilde{\mathbf{y}}_k - \mathbf{A}_k \text{vec}\left(\overline{\mathbf{Z}_k}\right) \in \mathbb{R}^{M_k \times 1}$ and $\mathbf{B}_k = \left(\mathbf{B}_k^{cc} \otimes \mathbf{B}_k^{sp}\right) \in \mathbb{R}^{NP \times NP}$.

Using $\mathbf{y}_k$ and dictionary matrix $\mathbf{A}_k \mathbf{B}_k$, estimate of joint sparse signal, $\widehat{\mathbf{x}}_k \in \mathbb{R}^{NP \times 1}$, is computed using the SBL framework [33]. The estimate $\widehat{\mathbf{X}}_k$ is computed using relation $\widehat{\mathbf{x}}_k = \text{vec}\left(\widehat{\mathbf{X}}_k\right)$ and the estimate of spatial matrix is then obtained as $\widehat{\mathbf{Z}}_k = \mathbf{B}_k \widehat{\mathbf{X}}_k + \overline{\mathbf{Z}_k}$. Note that correct calculation of $\text{vec}\left(\overline{\mathbf{Z}_k}\right)$ directly affects the joint recovery process.

V. Results and Discussions

This section illustrates the energy efficiency of the proposed multi-sensing strategies over the closest monolithic scheme proposed by Chen *et al.* in [14], [15], Silvestri *et al.* in [21], and Jain *et al.* in [16] on both synthetic and real data-sets. The scheme in [14], [15] is chosen because it developed subset selection strategy for optimized sensing, that in [21] developed heuristic-based sensor selection approaches (Top-W, Top-W-Update, and Batch selection), while the scheme in [16] proposed a method for random sensor selection and joint recovery of the WSN parameter signals. For fair comparison, SBL-based recovery scheme, EH-capability, and BCRB measure are included in the comparing schemes as well.

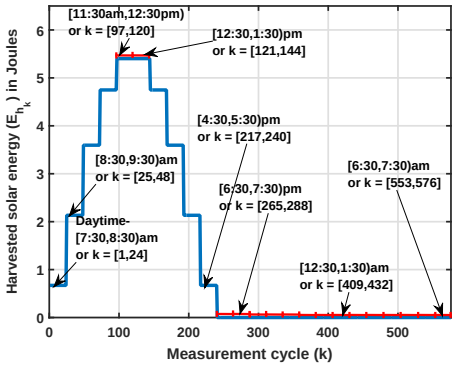

Fig. 3: Solar energy harvested by nodes during a day.

For the WSN considered in below sub-sections, the solar energy harvested by each node during different time of a day (576 measurement cycles; 1 cycle $\equiv$ 2.5 min [1]) corresponding to D_h (given in Section II-B) is shown in Fig. 3. The considered EH-WSN with the proposed multi-sensing strategies is simulated in Matlab.

A. Performance studies with synthetic data-set

$N = 80$ solar energy harvesting wireless nodes are considered deployed in a 2-dimensional WSN field of size 100×100 m^2 divided into $\lceil\sqrt{N}\rceil \times \lceil\sqrt{N}\rceil = 9 \times 9$ square areas of size $\approx 11 \times 11$ m^2 each, having one randomly deployed node [39]. The field is partitioned into $R = 4$ non-overlapping coverage regions designated by sets $\mathcal{R}_r, \forall 1 \leq r \leq R$, containing nodes within them. Initial energy is set as $E_{rem_0}(n) = 10$ J, $\forall 1 \leq n \leq N$. Considering multi-sensing for pollution monitoring application, each node is considered to have $P = 7$ sensors for monitoring CO, SO_2, NO_2, Cl_2, CH_4, NH_3, and H_2S pollutants. Their sensing energies are set as $\{E_s^p, 1 \leq p \leq P\} = \{0.6426, 1.3590, 1.5789, 1.4257, 0.3507, 0.9401, 1.9355\}$ J [31] and detection limits $\{\rho^p, 1 \leq p \leq P\} = \{0.02, 0.009, 0.01, 0.007, 0.015, 0.022, 0.015\}$. The detection limits considered here lie within dynamic range of synthetically generated pollutant signals. In practice, these are set as specified in sensors data-sheets. The p^{th} parameter signal across different nodes is obtained as $z_k^p(n) = \sum_{s=1}^{S^p} e^{-\frac{d_{n,s}}{\theta^p}} u_k^p(s)$ [20], where S^p is the total number of sources of p^{th} parameter (set as 1 here), $d_{n,s}$ is distance between n^{th} node and s^{th} source, θ^p represents spatial diffusion parameter, and $u_k^p(s)$ denotes random signal emitted from the s^{th} source of pollutant p during k^{th} measurement cycle. Temporal samples of the source signal $u_k^p(s)$ are generated using AR(1) process [20] as $u_{k+1}^p(s) = \varphi^p u_k^p(s) + \sqrt{1-(\varphi^p)^2} w_{k+1}^p(s)$, where φ^p denotes temporal correlation between two adjacent

samples of $u^p_{(\cdot)}(s)$, $w^p_{k+1}(s) \sim \mathcal{N}\left(0, \sigma^2_{u^p_k}(s)\right)$, and $\sigma^2_{u^p_k}(s)$ denotes the variance of $u^p_k(s)$. Cross-correlation among the pollutants is modeled using AR(1) process [40] as: $u^{p+1}_k(\cdot) = \varphi_{cc} u^p_k(\cdot) + \sqrt{1-(\varphi_{cc})^2} v^{p+1}_k(\cdot)$, where φ_{cc} represents cross-correlation between the pollution signals $u^p_k(\cdot)$ and $u^{p+1}_k(\cdot), \forall\ p$ and $v^{p+1}_k(s) \sim \mathcal{N}\left(0, \sigma^2_{u^p_k}(s)\right)$. The $p = 1$ pollution signal from each source in 1^{st} cycle is generated as $u^1_1(s) \sim \mathcal{N}(0,1),\ \forall s$ [41]. Each pollutant sources are located randomly in the WSN field. The spatio-temporal and cross correlation parameters are set as $\{\theta^p, 1 \le p \le P\} = \{100, 500, 1000, 5000, 200, 2000, 4000\}$, $\{\varphi^p, 1 \le p \le P\} = \{0.99, 0.92, 0.95, 0.98, 0.97, 0.96, 0.94\}$, and $\varphi_{cc} = 0.8$. The FC is located at 110 m above and 200 m away from field center. Noise variance is set as $\sigma^2 = 10^{-5}$, so as to guarantee reasonable sensing performance in the considered severely ill-posed estimation scenarios $(N/M^p_k \gg 2, \forall p), (NP/M_k \gg 2)$. Performance measures used are, network residual energy in k^{th} cycle $= \sum_{n=1}^{N} E_{rem_k}(n)$ and sensing error (nMSE)$= \frac{\left\|\mathbf{z}^p_k - \widehat{\mathbf{z}}^p_k\right\|^2}{\left\|\mathbf{z}^p_k\right\|^2}$. It gauges the energy in error against that in signal. The parameter Δ in MBS [20] is fixed as 10^{-8}. Unless otherwise specified, the BCRB window is set as $[\alpha, \beta] = \left[5 \times 10^{-5}, 5 \times 10^{-4}\right]$, according to minimum and maximum value of BCRB obtained in the comparing schemes. Note that, the BCRB is used because the MSE cannot be computed at the receiver due to unknown $\mathbf{z}^p_k$. The MSE plots are used to highlight stable sensing quality provided by the proposed framework. While solving (5), the objective functions are normalized using their respective smallest values- $\frac{\mathrm{Tr}\left\{\left(\frac{1}{\sigma^2}\left(\mathbf{B}^p_{k+1}\right)^T \widetilde{\mathbf{A}}^p_{k+1} \mathbf{B}^p_{k+1} + \left(\mathbf{\Gamma}^p_{k+1}\right)^{-1}\right)^{-1}\right\}}{\mathrm{Tr}\left\{\left(\frac{1}{\sigma^2}\left(\mathbf{B}^p_{k+1}\right)^T \mathbf{I}_N \mathbf{B}^p_{k+1} + \left(\mathbf{\Gamma}^p_{k+1}\right)^{-1}\right)^{-1}\right\}}$, $\frac{\left(\sum_{n=1}^{N} \frac{1}{E_{rem_k}(n)} \widetilde{\mathbf{A}}^p_{k+1}(n,n)\right)}{\left(\sum_{n \in \mathcal{E}} \frac{1}{E_{rem_k}(n)} \widetilde{\mathbf{A}}^p_{k+1}(n,n)\right)}$, where $\mathcal{E}$ is the set containing R nodes with the highest remaining energy. Signal estimates are averaged over 300 Monte-Carlo iterations in each measurement cycle. To effectively capture the dynamics of all pollutants (or parameter signals), the thresholds are heuristically set as $\{\delta^p_{th}, \forall p\} = \{0.1097, 0.3019, 0.2620, 0.1560, 0.1936, 0.2302, 0.2801\}$, $\{\epsilon^p_{th}, \forall p\} = \left\{2.5 \times 10^{-5}, \forall p\right\}$, and $\zeta = 0.1$. The initial training set $\mathcal{T}^p$ contains $K_{tr} = 5$ instances of the respective pollutant signals $\mathbf{z}^p_{(\cdot)}$. The multi-sensing strategy MS-SP retrain uses 2 instances of the signals $\mathbf{z}^p_{(\cdot)}, \forall\ p$.

TABLE III: Energy efficiency of the proposed strategies

(Synthetic data) Strategies	Energy consumption per cycle (J)	Energy efficiency(%)
Chen	109.3209	–
MS	70.3940	35.6078*
MS-SP	56.6233	48.2045*
MS-SP retrain	79.5577	27.2255*
iDEG	133.4718	–
MS-CC	66.3297	50.3042**

* – with respect to Chen [14], [15], ** – with respect to iDEG [16]

The power model of Mica2 mote [31], [42] is considered in this work for simulating the energy consumption aspect. Power consumed by the CPU, memory, and radio in different modes are set as $P_{memory(read)} = 3\text{V} \times 6.2\text{mA}, P_{memory(write)} = 3\text{V} \times 18.4\text{mA}, P_{memory(sleep)} = 3\text{V} \times 2\mu\text{A}, P_{CPU(active)} = 3\text{V} \times 8\text{mA}, P_{CPU(sleep)} = 3\text{V} \times 10\mu\text{A}, P_{radio(transmit)} = 3\text{V} \times 21.5\text{mA}, P_{radio(receive)} = 3\text{V} \times 7\text{mA}$, and $P_{radio(sleep)} = 3\text{V} \times 1\text{mA}$. 3V is voltage supplied to the Mica2 mote. In sensing operation, time taken by an active sensor to sense is set as 30 s (average response time of sensor [31]), and the same value is considered as sleeping duration of sleeping sensors, CPU, memory, and radio components (for synchronization in sensing). Further, it is assumed that a sensed signal sample is 2 bytes long. Time taken by memory to read and write 1 byte of data are set as 565 μs and 12.9 ms, respectively. Bit rate of the radio component with the Mica2 mote in the works [31], [42] is set as 76.8 kbits/s $= 9.6$ kbytes/s. Thus, time taken by the radio component to transit/receive 1 byte of data is: $\frac{1}{9.6\text{k}}$ s. Sleep duration of different components of the mote during different operations depend on the maximum time taken by any component in required mode to perform the operation. For transmitting data, it is assumed that a node transmits $(7 + 2 \times (\#\text{active sensors}))$ bytes long packet to the mobile robot, including 7 bytes overhead. The associated energies are computed as product of power and time consumed.

1) Performance comparison of MS and MS-SP strategies with state-of-the-art: Performance of the proposed multi-sensing strategies MS and MS-SP is compared with the closest monolithic approach developed by Chen *et al.* [14], [15] by running it separately for all the P pollutants. The monolithic approach by Chen is chosen because there exists no other strategy in literature that deals with subset selection for optimal multi-sensing and parameter estimation. From Fig. 4(a), it can be observed that the proposed strategies are more energy-efficient compared to the Chen's scheme. Using the proposed strategies, the heterogeneous WSN sustains throughout a day (i.e. considered 576 measurement cycles) even when there is no energy harvested from $241^{st} - 576^{th}$ cycle as seen from Fig. 3. While using Chen's scheme, it suffers from network outage (i.e. 0 network residual energy) in measurement cycles $427 - 576$ due to which sensing operation cannot be carried out. Table III captures values of energy consumption per cycle (E_{cons}) of the proposed and Chen's strategies and energy-efficiency with respect to Chen $(= \frac{|E_{cons;Chen} - E_{cons;MS}|}{E_{cons;Chen}} \times 100\%)$. This gain in energy efficiency in the proposed strategies is due to adaptive and optimized selection of each type of sensors while providing stable sensing quality as illustrated in Figs. 4(b)-(c). Similar sensing quality is achieved for other parameters as well. Low nMSE values (approximately $< 10^{-2}$) are achieved due to optimized multi-sensing based on chosen BCRB window $[\alpha, \beta]$ and using an efficient recovery technique SBL. Increasing trend in network residual energy in Fig. 4(a) is due to considered harvested energy profile Fig. 3.

Integrating retraining logic with the MS-SP strategy consumes more energy as observed from Fig. 4(a). However, this retraining prevents deterioration of the MSE in Figs. 4(b)-(c). Thus, it provides more stable sensing quality. For more insights

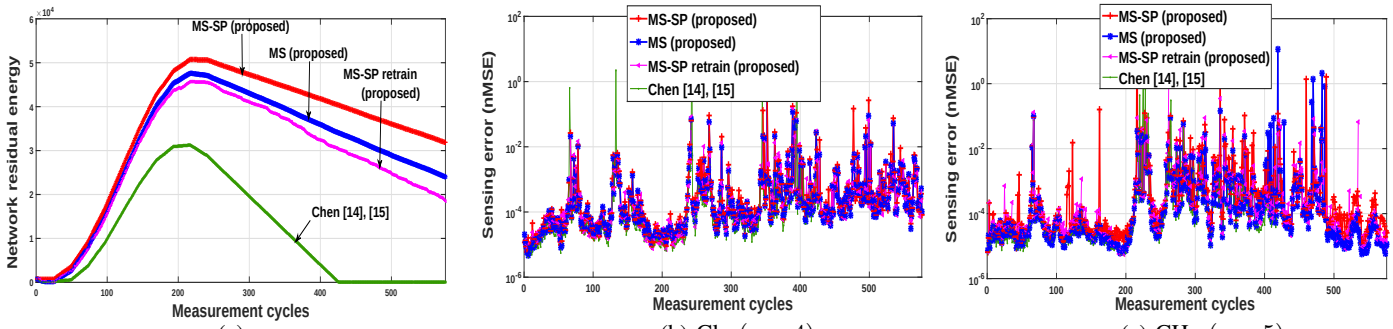

(a) (b) Cl_2 $(p = 4)$ (c) CH_4 $(p = 5)$

Fig. 4: Comparison of (a) network residual energy and (b-c) sensing error in $4^{th}, 5^{th}$ parameters estimates obtained using the proposed strategies (MS, MS-SP, and MS-SP retrain) with Chen's approach [14], [15] $(\{M_k^p, \forall p\} = \{15, 17, 18, 19, 16, 18, 19\}, \forall k)$.

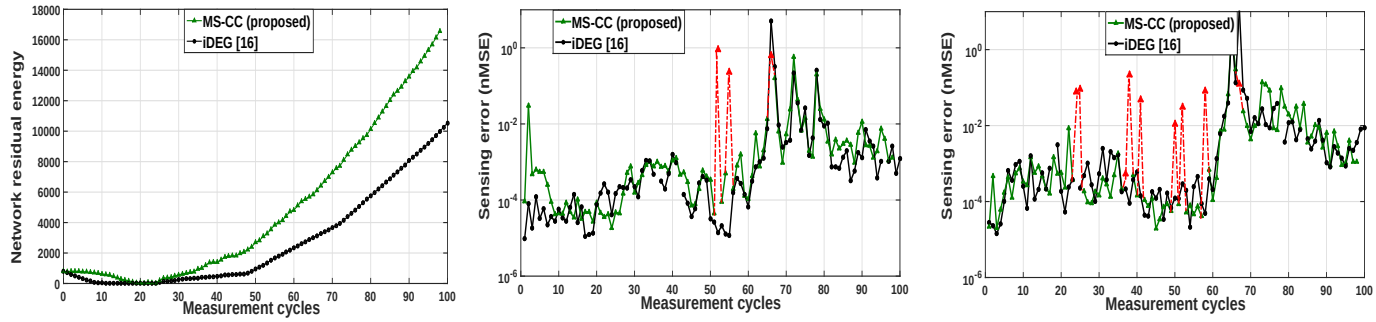

(a) (b) Cl_2 $(p = 4)$ (c) CH_4 $(p = 5)$

Fig. 5: (a) Network residual energy and (b-c) sensing error $\left(4^{th}, 5^{th}\right.$ parameters$\left.\right)$ comparison of the proposed strategy (MS-CC+joint recovery) with iDEG approach [16] $(\{M_k^p, \forall p\} = \{15, 17, 18, 19, 16, 18, 19\}, \forall k)$.

on retraining, refer Section V-A3.

Note that, discontinuities are observed in the nMSE curves of the proposed strategies. This is because estimation is not possible in some measurement cycles as either the parameter signal across corresponding sensors of all the nodes is below their detection limit or none of these sensors are active. While in Chen's case, it is due to no sensing and estimation operation because of network energy outage.

Remark 1: *The proposed strategies MS, MS-SP offer energy-efficient multi-sensing of slowly-varying correlated parameters in heterogeneous EH-WSN, thereby improving on energy sustainability of the nodes.*

2) Performance comparison of cross-correlation based sensing and joint recovery: To compare performance of the proposed MS-CC+joint recovery and the existing iDEG [16] strategy, joint recovery process is kept identical in both. For each pollutant/parameter, iDEG scheme chooses fixed number of sensors randomly in each cycle without exploiting correlation among them. The proposed one chooses them by suitably trading-off the sensing quality and energy efficiency, and exploiting cross-correlation among parameters. Figs. 5(a)-(c) and Table III indicates that the proposed strategy offers energy-efficient multi-sensing without affecting the sensing accuracy compared to the iDEG scheme.

Note that in the proposed MS and MS-SP multi-sensing strategies, sensor selection and signal estimation in $(M_k^p \times N)$ dimension space for each parameter/signal type are required to run in parallel in each measurement cycle. To analyze the results, we ran these tasks sequentially in Matlab in each measurement cycle. This increases computation time per cycle by $\sim P$ (7 here) times. Likewise, for MS-CC strategy, we ran sensor selection task sequentially and then performed joint signal estimation task in $\left(\sum_{p=1}^{P} M_k^p \times NP\right)$ dimension space. Further, to adapt the number of active sensors of each type for next cycle, joint estimation task is repeated to find signal estimates using pruned active sets. Thus, computation time increased here as well. Due to this, ~ 100 measurement cycles are considered while simulating results shown in Figs. 5(a-c) and in subsequent sections. Further, the increasing trend in Fig. 5(a) is due to the considered harvested energy profile shown in Fig. 3. For further measurement cycles, this plot shows behavior similar to the plot in Fig. 4(a), i.e. first increasing and then decreasing when there is no harvested energy during evening time. Usually, dimensioning of solar panels (used with the wireless node) is done such that the harvested energy profile and node's energy consumption in sensing, communication, etc. operations result in stable remaining energy of the node and the network. In our case, network's remaining energy first increases, then decreases; the trend will be followed for further measurement cycles because of the energy harvesting cycles. Design/dimensioning of the solar cells/panel [43] for achieving a stable network remaining

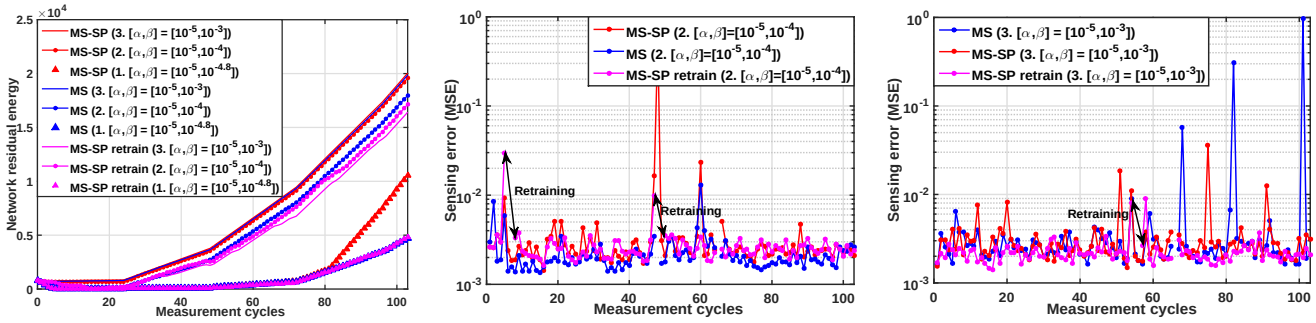

(a) (b) NO_2 $(p = 3)$ (c) Cl_2 $(p = 4)$

Fig. 6: Effects of retraining: (a) residual energy, (b-c) sensing quality $\left(3^{rd}, 4^{th}\right.$ parameter$\left.\right)$ for different BCRB windows $[\alpha, \beta]$.

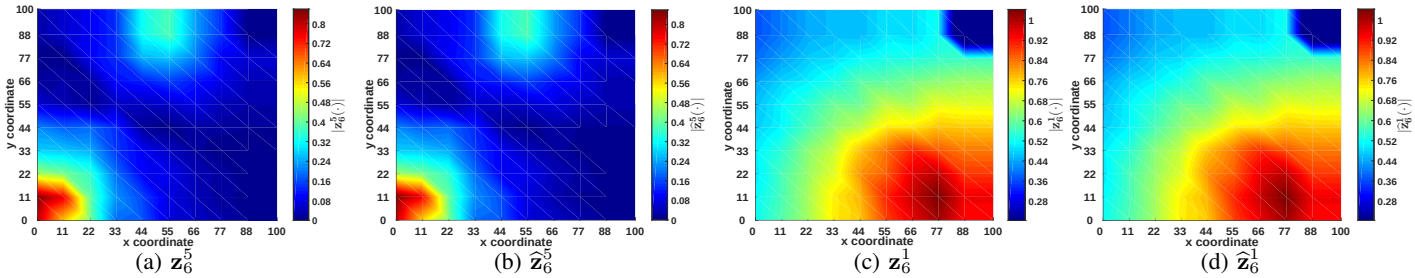

(a) $\mathbf{z}_6^5$ (b) $\widehat{\mathbf{z}}_6^5$ (c) $\mathbf{z}_6^1$ (d) $\widehat{\mathbf{z}}_6^1$

Fig. 7: Heat-maps of actual and estimated multi-source pollution signal (a) $\mathbf{z}_6^5$, (b) $\widehat{\mathbf{z}}_6^5$ and single-source signal (c) $\mathbf{z}_6^1$, (d) $\widehat{\mathbf{z}}_6^1$.

energy is out of scope of this work.

3) Retraining: For the three considered BCRB windows $([\alpha, \beta])$- 1. narrow $(= \left[5 \times 10^{-5}, 5 \times 10^{-4.8}\right])$, 2. moderate $(= \left[5 \times 10^{-5}, 5 \times 10^{-4}\right])$, and 3. wide $(= \left[5 \times 10^{-5}, 5 \times 10^{-3}\right])$, it can be observed from Fig. 6(a) that as the BCRB window widens (i.e. case 1→2→3), the energy efficiency of the MS and MS-SP strategies increase. While for the MS-SP retrain strategy, it is not so because relaxing BCRB in case 3 results in relatively more acceptable/tolerable error ⇒ frequent retraining compared to the case 2.

Further, energy efficiency-wise the MS-SP performs better than the MS-SP retrain scheme in all 3 cases. As the BCRB window tightens, the MS-SP retrain strategy performs better than and closer to the MS strategy. In BCRB case 2, MS-SP retrain undergoes less frequent retraining than BCRB case 3 due to which gap between MS-SP and MS-SP retrain, MS and MS-SP retrain increase for case 3 compared to case 2.

Sensing quality-wise, the MS-SP retrain scheme performs better than both MS and MS-SP strategies due to retraining as illustrated for cases 2 and 3 in Figs. 6(b),(c) respectively. For case 1 (stricter BCRB), it was observed in simulations that all 3 strategies provide similar sensing quality. Note that, here MSE $= \|\mathbf{z}_k^p - \widehat{\mathbf{z}}_k^p\|^2$ is used to quantify the sensing quality as effect of retraining is more clearly observed in these MSE plots than the nMSE plots.

Remark 2: *Retraining improves the sensing quality at the cost of energy efficiency.*

4) Multi-sensing in a WSN field with multiple sources: A generic pollution monitoring WSN field now considered with more than one source of different pollutants $(S^p > 1)$ generating pollution signals. Number of sources of each pollutant are set as $\{S^p, \forall p\} = \{1, 2, 1, 1, 2, 1, 2\}$. X and Y coordinates (in m) of randomly generated locations of the pollutants with multiple sources, i.e. SO_2, CH_4, and H_2S, are respectively $\left\{(x_{s^2}^2, y_{s^2}^2), 1 \leq s^2 \leq S^2\right\} = \{(11, 12), (77, 88)\}$, $\left\{(x_{s^5}^5, y_{s^5}^5), 1 \leq s^5 \leq S^5\right\} = \{(10, 15), (55, 95)\}$, and $\left\{(x_{s^7}^7, y_{s^7}^7), 1 \leq s^7 \leq S^7\right\} = \{(96, 80), (20, 5)\}$. Various thresholds are set as $\{\delta_{th}^p, \forall p\} = \{0.1177, 0.3106, 0.2451, 0.1492, 0.1890, 0.2249, 0.2747\}$, $\{\rho^p, \forall p\} = \{0.2651, 0.02, 0.03, 0.01, 0.08, 0.02, 0.025\}$. Sensing energy parameters are set as $\{E_s^p, \forall p\} = \{0.5621, 1.2238, 1.6390, 1.7433, 0.2883, 1.2749, 1.9042\}$ J. Rest spatial, temporal, and cross correlation parameters are kept same as in above sections.

From heat-maps of actual and estimated signals in Figs. 7(a)-(d), it can be observed that there are two sources of the 5^{th} pollutant (near actual location $(10, 15)$ m and $(55, 95)$ m) and one source of the 1^{st} pollutant. Thus, the proposed strategies can effectively sense and estimate signals in multi-source monitoring scenarios as well without loss of sensing accuracy. nMSE in estimates of multi-source CH_4 signal $(\widehat{\mathbf{z}}_k^5)$ and single-source CO signal $(\widehat{\mathbf{z}}_k^1)$ in measurement cycle $k = 6$ are respectively 0.0013 and 0.00052 for MS strategy.

Multi-source sparse sensing and estimation ability of the proposed energy-efficient multi-sensing strategies have immense practical applicability in the following IoT applications- 1. air quality monitoring (classification of the observing field in different zones based on severity of estimated pollution signals), 2. gas leakage detection, 3. source localization.

5) Effect of imperfect knowledge of harvested energy: This section investigates behavior of the proposed framework with imperfect knowledge of the harvested/arriving energy. For this, a WSN field (100×100) m^2 with $N = 32$ randomly deployed nodes, each having $P = 4$ sensors mounted on them is

TABLE IV: Effect of error in prediction of harvested energy

$\frac{\Delta E_h}{E_{rem}(\cdot)}$	$\frac{\Delta E_h}{E_h}$	$\mathcal{A}_k^1$	$\mathcal{A}_k^2$	$\mathcal{A}_k^3$	$\mathcal{A}_k^4$
$\frac{0}{10}$ (no error)	$\frac{0}{0.6709}$	$\{1,2,3,4,5,6,7,8,10,22,25,26,27\}$	$\{1,7,10,22,26,27,29,30,31,32\}$	$\{1,10,22,24,26,27,29,30,31,32\}$	$\{1,7,10,22,24,26,29,30,31,32\}$
$\frac{0.3354}{10}$	0.5	$\{1,2,3,4,5,6,7,8,10,22,25,26,27\}$	$\{1,7,10,22,26,27,29,30,31,32\}$	$\{1,10,22,24,26,27,29,30,31,32\}$	$\{1,7,10,22,24,26,29,30,31,32\}$
$\frac{0.6}{10}$	0.8943	$\{1,2,3,4,5,6,7,8,10,22,25,26,27\}$	$\{1,7,10,22,26,27,29,30,31,32\}$	$\{1,10,22,24,26,27,29,30,31,32\}$	$\{1,7,10,22,24,26,29,30,31,32\}$
$\frac{2.5}{10}$	3.7263	$\{1,2,3,4,5,6,7,8,10,22,25,26,27\}$	$\{1,7,10,22,26,27,29,30,31,32\}$	$\{1,10,22,24,26,27,29,30,31,32\}$	$\{1,7,10,22,24,26,29,30,31,32\}$
$\frac{5}{10}$	7.4527	$\{1,2,3,4,5,6,7,8,10,17,25,26,27\}$	$\{1,7,10,22,26,27,29,30,31,32\}$	$\{1,10,15,22,24,26,29,30,31,32\}$	$\{1,7,10,22,24,26,29,30,31,32\}$
$\frac{10}{10}$	14.905	$\{1,2,3,4,5,6,7,8,10,17,25,26,27\}$	$\{1,7,10,22,25,26,27,30,31,32\}$	$\{1,10,15,19,22,24,29,30,31,32\}$	$\{1,7,10,22,24,26,29,30,31,32\}$

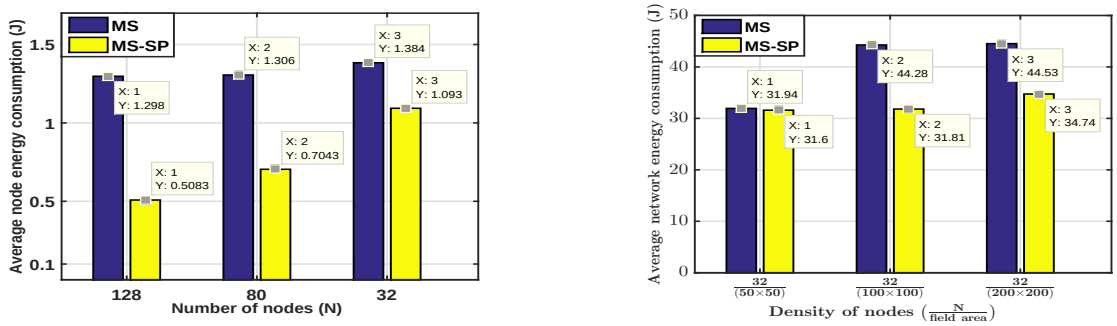

Fig. 8: (a) Average node energy consumption versus number of nodes and (b) average network energy consumption versus density of nodes of the proposed strategies: MS and MS-SP.

simulated. Initial energy of the nodes is set as $E_{rem_0}(n) = 10$ J, $1 \leq n \leq N$. P synthetic signals are generated and other parameters are set as discussed in Section V-A of the manuscript. Error introduced in the energy harvested by each node is denoted by ΔE_h. This error could be due to imperfect knowledge of the harvested energy or error in its prediction at the FC. The difference in active sets $(\mathcal{A}_k^p, \forall p)$ obtained by running the relaxed MOP (6) for different values of $\frac{\Delta E_h}{E_{rem}(\cdot)}$ is observed, where $E_{rem}(\cdot)$ represents remaining energy of a node. Here, the subscript k is dropped for brevity. From Table IV it can be observed that, as the ratio $\frac{\Delta E_h}{E_{rem}(\cdot)}$ increases (approaches 0.5 or higher values) or the prediction error $\frac{\Delta E_h}{E_h}$ increases, the active sets $(\mathcal{A}_k^p, \forall p)$ obtained in presence of error differ from the case when there is no error. While for the lower values of $\frac{\Delta E_h}{E_{rem}(\cdot)}$ (< 0.5), the active sets obtained are same in both the cases. The entity E_h represents actual harvested energy and is set as 0.6709 for all the nodes in the considered measurement cycle.

6) Effect of number and density of nodes on energy consumption: A simulation scenario is considered where the WSN field spans 100×100 m^2 area with randomly deployed nodes N each having $P = 4$ sensors to sense different parameters. Initial energy of the nodes is set as $E_{rem_0}(\cdot) = 10$ J. Their sensing energies are set as $\{E_s^p, \forall p\} = \{0.6324, 1.3328, 1.5761, 1.4249\}$ J. P synthetic signals are generated as discussed in Section V.A (spatio-temporal characteristics corresponding to first four signals are used). Detection limits of the sensors are set as $\{\rho^p, \forall p\} = \{0.02, 0.019, 0.006, 0.0357\}$. Thresholds are set as $\{\delta_{th}^p, \forall p\} = \{0.1228, 0.2557, 0.2804, 0.1629\}$, $\{\epsilon_{th}^p, \forall p\} = \{2.5 \times 10^{-5}, \forall p\}$, and BCRB window is set as $[\alpha, \beta] = [5 \times 10^{-5}, 5 \times 10^{-3}]$. Energy consumption per node per measurement cycle (i.e., average node energy consumption) using the MS and MS-SP schemes are plotted against the number of nodes N in Fig. 8(a). It can be observed that average node energy consumption decreases with the increase in N for the same BCRB window. This is because correlation among measurement of the nodes increases, which allows effective field monitoring using even lesser number of sensor measurements and also gives more opportunity to collaborate at network level. Further, it can also be verified that the MS-SP scheme consumes less energy compared to the MS scheme. Likewise, by decreasing field area while keeping N fixed, it can be observed from Fig. 8(b) that, as the density of nodes $\left(\frac{N}{\text{field area}}\right)$ increases the average network energy consumption (i.e. network energy consumption per measurement cycle) decreases while maintaining the same BCRB window.

B. Performance studies with real WSN data-set

To compare performance of the proposed multi-sensing strategies with Chen's [14], [15], Silvestri's [21] (Top-W, Top-W-Update, Batch Selection), and iDEG [16] schemes using real data-set, comprised of temperature, humidity, light, and voltage, collected from a WSN deployed in Intel Berkeley research lab [44] is considered. These $P = 4$

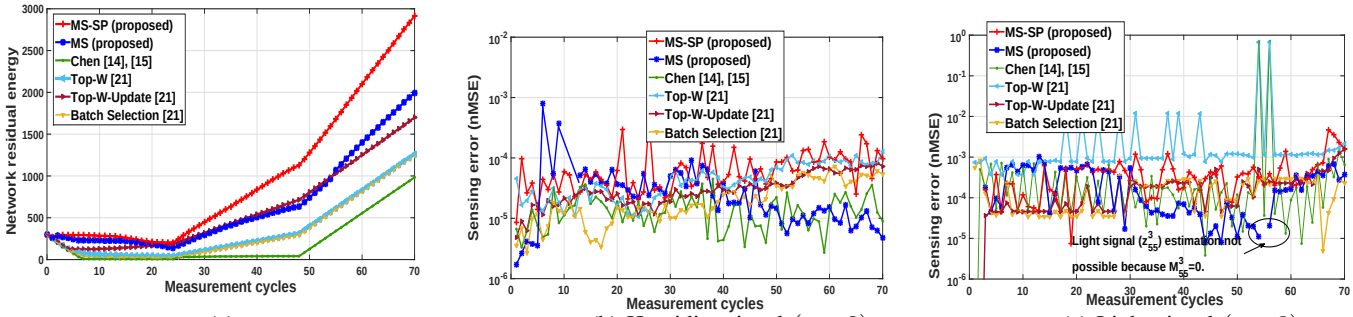

(a) (b) Humidity signal $(p = 2)$ (c) Light signal $(p = 3)$

Fig. 9: Comparison of the proposed strategies (MS and MS-SP) with Chen's approach [14], [15] and Silvestri's approaches [21] (Top-W, Top-W-Update, and Batch selection) with $\{M_k^p, \forall p\} = \{15, 16, 17, 18\}, \forall k$: (a) Network residual energy, (b) humidity sensing error, and (c) light sensing error.

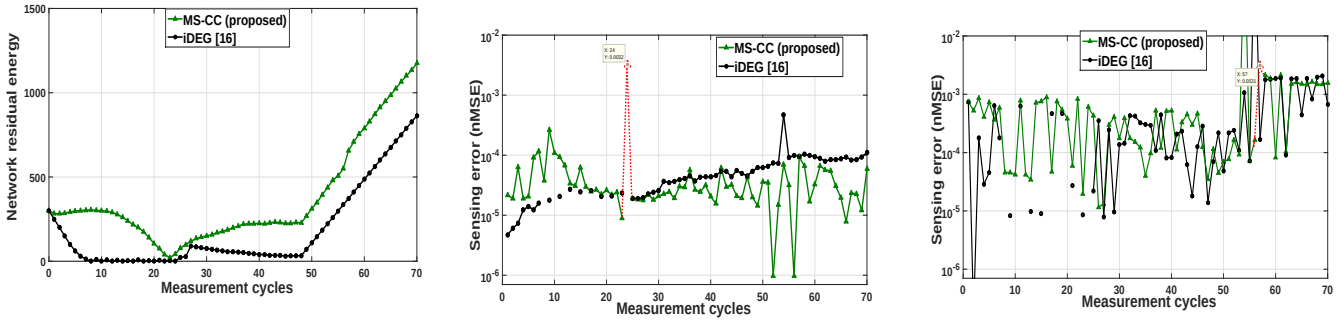

(a) (b) Humidity signal $(p = 2)$ (c) Light signal $(p = 3)$

Fig. 10: Comparison of (a) network residual energy and (b-c) sensing error in estimates of humidity signal $(p = 2)$ and light signal $(p = 3)$ obtained using the proposed strategy (MS-CC+joint recovery) with iDEG approach [16] $(\{M_k^p, \forall p\} = \{15, 16, 17, 18\}, \forall k)$.

correlated signals sensed by a subset of 30 Mica2Dot sensors spanning over 25×32 m^2 lab area are considered. Parameters $\{[\alpha^p, \beta^p], \forall p\}, \delta_{th}^p, \epsilon_{th}^p, R, \rho^p$, and σ^2 are respectively set as $\{[1.0249 \times 10^{-6}, 0.0522], [3.0683 \times 10^{-6}, 0.0522], [2.04654297 \times 10^{-6}, 0.0522], [2.0469 \times 10^{-6}, 0.0522]\}$, $\{0.0595, 0.0627, 0.4178, 0.0174\}, \{0.5, 0.5, 0.05, 0.05\}, 4$, $\{14.4, 38.6, 1.1, 2.24\}$, and $\sim 10^{-6}$. The energy parameters are set as $E_{rem_0}(n) = 10$ J, $\forall n$ and $\{E_s^p, 1 \leq p \leq P\} = \{0.6426, 1.3590, 1.5789, 1.4257\}$ J. In practice, the sensing energy of different sensors are set as specified in their data-sheets. Here, their values are set comparable to the initial energy of the nodes so as to analyze results effectively. Rest all the parameters are similar to the synthetic case. Fig. 9(a) and Fig. 10(a) validate that the proposed multi-sensing strategies MS, MS-SP, and MS-CC are indeed more energy-efficient compared to Chen's approach, Silvestri's approaches, and iDEG scheme respectively. Energy efficiency of MS, MS-SP with respect to Chen's and Silvestri's schemes and that of MS-CC with respect to iDEG scheme are presented in Table V. Due to the considered profile of energy harvesting (Fig. 3), Fig. 4(a) (using synthetic data) shows increasing trend in network residual energy for cycles till the energy harvested is increasing; thereafter a decreasing trend in residual energy is observed when the energy harvested decreases and becomes 0. For the results with real-data set, for simplicity of demonstration the network residual energy performance is simulated for 70 measurement cycles during day-time when the rate of harvested energy is high. The trends are similar to that observed in Fig. 4(a) for the different schemes. For the remaining cycles when energy harvested decreases or becomes 0, reduction in network residual energy is expected, with the MS-SP having a slower decreasing rate. Further, from Figs. 9(b)-(c) and Figs. 10(b)-(c), it can be verified that the order of sensing quality has not been changed significantly to achieve this gain in energy efficiency. For instance, the average values of nMSE for humidity signal $\{7.6, 4.09, 1.48, 4.86, 3.38, 2.42\} \times 10^{-5}$ (Fig. 9(b)), obtained respectively using MS-SP, MS methods, and Chen's, Top-W, Top-W-Update, and batch selection schemes, are on the same order $(\sim 10^{-5}$ here$)$. A similar observation holds for light signal, in which the average nMSE values obtained for the different competitive schemes are $\{5.03, 2.42, 200, 214, 2.06, 1.67\} \times 10^{-4}$ (Fig. 9(c)). Similar sensing quality is achieved for parameters $p = 1$ and 4 i.e. temperature and voltage signals.

C. Advantage of joint recovery in MS-CC over individual recovery in MS/MS-SP

Exploiting cross-correlation in MS-CC+joint recovery scheme facilitates recovery of a parameter signal even if the

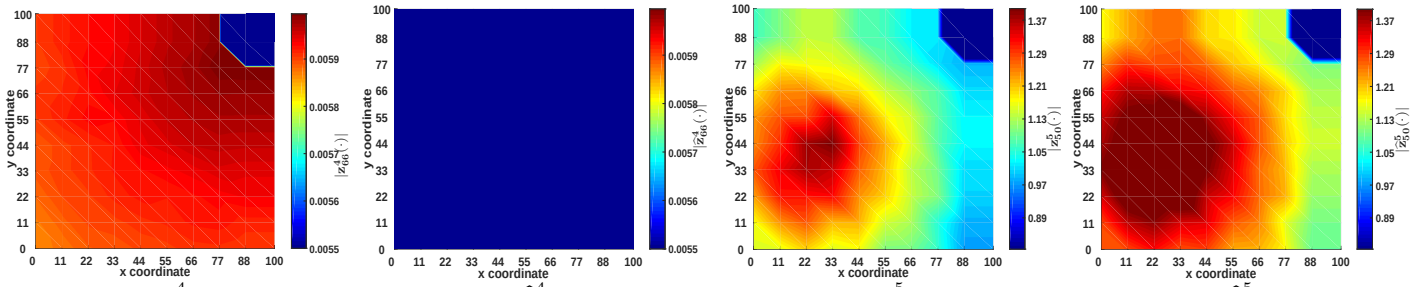

(a) $\mathbf{z}_{66}^4$ (b) $\widehat{\mathbf{z}}_{66}^4$ (c) $\mathbf{z}_{50}^5$ (d) $\widehat{\mathbf{z}}_{50}^5$

Fig. 11: Heat-maps of actual and estimated pollution signals (a) $\mathbf{z}_{66}^4$, (b) $\widehat{\mathbf{z}}_{66}^4$ obtained from MS-SP strategy, (c) $\mathbf{z}_{50}^5$ and (d) $\widehat{\mathbf{z}}_{50}^5$ obtained from MS-CC strategy using synthetic data.

TABLE V: Energy efficiency of the proposed strategies

(Real data-set) **Strategies**	**Energy consumption per cycle (J)**	**Energy efficiency**(%)
Chen	52.9793	–
Top-W	49.0074	–
Top-W-Update	42.7419	–
Batch Selection	49.1497	–
MS	38.5451	$27.2449^{*}, 21.3484^{+}$ $9.8189^{++}, 21.5761^{+++}$
MS-SP	25.3792	$52.0959^{*}, 48.2135^{+}$ $40.6221^{++}, 48.3634^{+++}$
iDEG	54.6816	–
MS-CC	50.2347	8.1323^{**}

* – with respect to Chen [14], [15], ** – with respect to iDEG [16], $^{++}$ – with respect to Top-W-Update [21], $^{+++}$ – with respect to Batch Selection [21], $^{+}$ – with respect to Top-W [21].

corresponding sensors of all N nodes are sleeping. While this is not possible in case of MS/MS-SP+individual sparse recovery of parameters. Dotted nMSE lines across 24^{th} cycle in Fig. 10(b) and 57^{th} cycle in Fig. 10(c) show that the humidity and light signals are estimated with the nMSE values 0.0032 and 0.0031 even when corresponding sensors of all the field nodes did not participate in sensing (i.e. $M_{24}^2 = M_{57}^3 = 0$). However, Fig. 9(c) illustrates that using MS+individual recovery, it is not possible to recover $p = 3$ light signal in 55^{th} cycle when $M_{55}^3 = 0$. Similar behavior is seen for simulations using synthetic case in Sections V-A1 and V-A2. Here, in the MS-SP strategy $M_{66}^4 = 0$, due to which $\widehat{\mathbf{z}}_{66}^4$ is not estimated as seen in Figs. 11(a-b) showing heat-maps of actual and estimated signals of type 4. While in MS-CC, even though $M_{50}^5 = 0$, $\widehat{\mathbf{z}}_{50}^5$ is still estimated as seen from the heat-maps of actual and estimated type 5 signals in Figs. 11(c-d).

Remark 3: *Cross-correlation based sensing and estimation help in estimating a sensor's signal without the actual measurements from the corresponding sensors.*

VI. Conclusion

This paper has proposed novel energy-efficient adaptive multi-sensing strategies (MS, MS-SP, and MS-CC) in energy harvesting heterogeneous WSN. The strategies adaptively activate a subset of sensors of a few field nodes to monitor different correlated parameter signals. To do so, sensing quality and energy efficiency of the WSN are jointly optimized for each parameter, and the inherent spatial, temporal, and cross-correlation among them are exploited for further adaptation and pruning of the active sensors sets. Energy consumption of different components of a node has been integrated in the formulation which is often ignored in the literature. Further, system constraints due to different detection limits of the sensors and stochastic solar energy availability have also been incorporated in the proposed strategies. A retraining logic has also been developed that detects the need for retraining a type of sensors in current measurement cycle to prevent deterioration of the sensing quality. A SBL-based joint sparse recovery scheme using Kronecker product of PCA-based spatial and cross-correlation bases and MS-CC based active sensors' measurements has also been presented. It estimates a field parameter even if all the corresponding sensors are sleeping. Extensive simulation results on real data-sets have demonstrated that the proposed MS-SP strategy along with individual parameter recovery and MS-CC with joint recovery are respectively 52% and 8% more energy-efficient compared to the closest subset selection and field recovery strategies.

References

[1] V. Gupta and S. De, "Adaptive multi-sensing in EH-WSN for smart environment," in *Proc. IEEE Global Commun. Conf. (GLOBECOM)*. Big Island, HI, USA, 2019.

[2] A. De Paola, P. Ferraro, S. Gaglio, G. L. Re, and S. K. Das, "An adaptive Bayesian system for context-aware data fusion in smart environments," *IEEE Trans. Mobile Comput.*, vol. 16, no. 6, pp. 1502–1515, 2017.

[3] J. M. Corchado, J. Bajo, D. I. Tapia, and A. Abraham, "Using heterogeneous wireless sensor networks in a telemonitoring system for healthcare," *IEEE Trans. Inform. Technol. Biomedicine*, vol. 14, no. 2, pp. 234–240, 2009.

[4] Z. Wang, J. Wu, J. Yang, and Y. Cao, "Optimum distributed estimation of a spatially correlated random field," *IEEE Trans. Signal Inform. Process. over Netw.*, vol. 5, no. 4, pp. 739–752, 2019.

[5] M. Hammoudeh, F. Al-Fayez, H. Lloyd, R. Newman, B. Adebisi, A. Bounceur, and A. Abuarqoub, "A wireless sensor network border monitoring system: Deployment issues and routing protocols," *IEEE Sensors J.*, vol. 17, no. 8, pp. 2572–2582, 2017.

[6] L. Gao, G. Battistelli, and L. Chisci, "Event-triggered distributed multi-target tracking," *IEEE Trans. Signal Inform. Process. over Netw.*, vol. 5, no. 3, pp. 570–584, 2019.

[7] K. Kaushik, D. Mishra, and S. De, "Stochastic solar harvesting characterization for sustainable sensor node operation," *IET Wireless Sensor Systems J.*, vol. 9, no. 4, pp. 208–217, 2019.

[8] Q. Ling and Z. Tian, "Decentralized sparse signal recovery for compressive sleeping wireless sensor networks," *IEEE Trans. Signal Process.*, vol. 58, no. 7, pp. 3816–3827, 2010.

[9] T. Xue, X. Dong, and Y. Shi, "Multiple access and data reconstruction in wireless sensor networks based on compressed sensing," *IEEE Trans. Wireless Commun.*, vol. 12, no. 7, pp. 3399–3411, 2013.

[10] Y. Chen and Q. Zhao, "On the lifetime of wireless sensor networks," *IEEE Commun. Lett.*, vol. 9, no. 11, pp. 976–978, 2005.

[11] S. Joshi and S. Boyd, "Sensor selection via convex optimization," *IEEE Trans. Signal Process.*, vol. 57, no. 2, pp. 451–462, 2009.

[12] S. Hwang, R. Ran, J. Yang, and D. K. Kim, "Multivariated Bayesian compressive sensing in wireless sensor networks," *IEEE Sensors J.*, vol. 16, no. 7, pp. 2196–2206, 2015.

[13] S. P. Chepuri and G. Leus, "Sparsity-promoting sensor selection for non-linear measurement models," *IEEE Trans. Signal Process.*, vol. 63, no. 3, pp. 684–698, 2015.

[14] W. Chen and I. J. Wassell, "Compressive sleeping wireless sensor networks with active node selection," in *Proc. IEEE Global Commun. Conf. (GLOBECOM)*. Austin, TX, USA, 2014, pp. 7–12.

[15] ——, "Optimized node selection for compressive sleeping wireless sensor networks," *IEEE Trans. Veh. Technol.*, vol. 65, no. 2, pp. 827–836, 2016.

[16] N. Jain, V. A. Bohara, and A. Gupta, "iDEG: Integrated data and energy gathering framework for practical wireless sensor networks using compressive sensing," *IEEE Sensors J.*, vol. 19, no. 3, pp. 1040–1051, 2018.

[17] P. Zhang, I. Nevat, G. W. Peters, F. Septier, and M. A. Osborne, "Spatial field reconstruction and sensor selection in heterogeneous sensor networks with stochastic energy harvesting," *IEEE Trans. Signal Process.*, vol. 66, no. 9, pp. 2245–2257, 2018.

[18] G. Quer, R. Masiero, G. Pillonetto, M. Rossi, and M. Zorzi, "Sensing, compression, and recovery for WSNs: Sparse signal modeling and monitoring framework," *IEEE Trans. Wireless Commun.*, vol. 11, no. 10, pp. 3447–3461, 2012.

[19] J. Hao, B. Zhang, Z. Jiao, and S. Mao, "Adaptive compressive sensing based sample scheduling mechanism for wireless sensor networks," *Pervasive and Mobile Comput.*, vol. 22, pp. 113–125, 2015.

[20] V. Gupta and S. De, "SBL-based adaptive sensing framework for WSN-assisted IoT applications," *IEEE Internet of Things J.*, vol. 5, no. 6, pp. 4598–4612, 2018.

[21] S. Silvestri, R. Urgaonkar, M. Zafer, and B. J. Ko, "A framework for the inference of sensing measurements based on correlation," *ACM Trans. Sensor Networks*, vol. 15, no. 1, p. 4, 2018.

[22] D. Bri, H. Coll, M. Garcia, and J. Lloret, "A multisensor proposal for wireless sensor networks," in *Proc. IEEE Int. Conf. Sensor Tech. and Appl. (SENSORCOMM)*. Cap Esterel, France, 2008, pp. 270–275.

[23] M. A. Akbar, A. A. S. Ali, A. Amira, M. Benammar, F. Bensaali, S. Mohamad, F. Tang, A. Bermak, M. Zgaren, and M. Sawan, "A multi-sensing reconfigurable platform for gas applications," in *Proc. IEEE Int. Conf. Microelec. (ICM)*. Doha, Qatar, 2014, pp. 148–151.

[24] M. V. Ramesh and V. P. Rangan, "Data reduction and energy sustenance in multisensor networks for landslide monitoring," *IEEE Sensors J.*, vol. 14, no. 5, pp. 1555–1563, 2014.

[25] R. Prabha, M. V. Ramesh, V. P. Rangan, P. Ushakumari, and T. Hemalatha, "Energy efficient data acquisition techniques using context aware sensing for landslide monitoring systems," *IEEE Sensors J*, vol. 17, pp. 6006–6018, 2017.

[26] C. R. Rao, "The use and interpretation of principal component analysis in applied research," *Sankhyā: The Indian J. Statistics, Ser. A*, pp. 329–358, 1964.

[27] M. Alnuaimi, K. Shuaib, K. Alnuaimi, and M. Abdel-Hafez, "Data gathering in delay tolerant wireless sensor networks using a ferry," *Sensors*, vol. 15, no. 10, pp. 25 809–25 830, 2015.

[28] F. Fan, G. Wu, M. Wang, Q. Cao, and S. Yang, "Robot delay-tolerant sensor network for overhead transmission line monitoring," *Applied Sciences*, vol. 8, no. 6, p. 847, 2018.

[29] Y. Yun, Y. Xia, B. Behdani, and J. C. Smith, "Distributed algorithm for lifetime maximization in a delay-tolerant wireless sensor network with a mobile sink," *IEEE Trans. Mobile Comput.*, vol. 12, no. 10, pp. 1920–1930, 2012.

[30] V. Gupta, S. Tripathi, and S. De, "Green sensing and communication: A step towards sustainable IoT systems," *Springer J. Indian Institute Sci.*, pp. 1–16, 2020.

[31] P. Gupta, K. Kandakatla, S. De, and S. Jana, "Feasibility analysis on integrated recharging and data collection in pollution sensor networks," in *Proc. Nat. Conf. Commun. (NCC)*. New Delhi, India, 2013, pp. 1–5.

[32] S. S. Chandel and R. K. Aggarwal, "Estimation of hourly solar radiation on horizontal and inclined surfaces in western himalayas," *Smart grid and renewable energy*, vol. 2, no. 01, p. 45, 2011.

[33] D. P. Wipf and B. D. Rao, "Sparse Bayesian learning for basis selection," *IEEE Trans. Signal Process.*, vol. 52, no. 8, pp. 2153–2164, Aug. 2004.

[34] I. CVX Research, "CVX: Matlab software for disciplined convex programming, version 2.0," http://cvxr.com/cvx, Aug. 2012.

[35] J. F. Hemphill, "Interpreting the magnitudes of correlation coefficients." *American Psychologist*, vol. 58, no. 1, pp. 78–80, 2003.

[36] Y. Zhang, "On extending some primal–dual interior-point algorithms from linear programming to semidefinite programming," *SIAM J. on Optimization*, vol. 8, no. 2, pp. 365–386, 1998.

[37] R. Masiero, G. Quer, D. Munaretto, M. Rossi, J. Widmer, and M. Zorzi, "Data acquisition through joint compressive sensing and principal component analysis," in *Proc. IEEE Global Telecommun. Conf. (GLOBECOM)*. Honolulu, HI, USA, 2009, pp. 1–6.

[38] K. B. Petersen, M. S. Pedersen *et al.*, "The matrix cookbook," *Technical University of Denmark*, vol. 7, p. 15, 2008.

[39] M. Leinonen, M. Codreanu, and M. Juntti, "Sequential compressed sensing with progressive signal reconstruction in wireless sensor networks," *IEEE Trans. Wireless Commun.*, vol. 14, no. 3, pp. 1622–1635, 2015.

[40] M. Blangiardo, M. Pirani, L. Kanapka, A. Hansell, and G. Fuller, "A hierarchical modelling approach to assess multi pollutant effects in time-series studies," *PloS one*, vol. 14, no. 3, p. e0212565, 2019.

[41] J. V. Zidek, W. Sun, and N. D. Le, "Designing and integrating composite networks for monitoring multivariate Gaussian pollution fields," *J. Royal Statistical Soc.: Ser. C*, vol. 49, no. 1, pp. 63–79, 2000.

[42] V. Shnayder, M. Hempstead, B.-r. Chen, G. W. Allen, and M. Welsh, "Simulating the power consumption of large-scale sensor network applications," in *Proc. Intl. Conf. Embedded networked sensor syst.* ACM, 2004, pp. 188–200.

[43] S. Suman and S. De, "Low complexity dimensioning of sustainable solar-enabled systems: A case of base station," *IEEE Trans. Sustain. Comput.*, pp. 1–17, 2020 (in press).

[44] P. Bodik, W. Hong, C. Guestrin, S. Madden, M. Paskin, and R. Thibaux, "Intel lab data," *Online dataset*, Feb. 2004.

Vini Gupta received the B.Tech. degree in Electronics and Communication Engineering from Indira Gandhi Institute of Technology, Guru Gobind Singh Indraprastha University, New Delhi, India, in 2013 and the M.Tech. degree in Signal Processing and Communication from the Department of Electrical Engineering, IIT Kanpur, Uttar Pradesh, India, in 2016. She worked in Tata Consultancy Services Limited, New Delhi, as an Assistant System Engineer, from 2013 to 2014. She is currently working toward the Ph.D. degree in the Department of Electrical Engineering, IIT Delhi, New Delhi, India. Her research interests include design of centralized and distributed green sensing framework for wireless sensor networks-based IoT applications, application of sparse signal processing and Bayesian learning for networked sensing, and radar signal processing. She is a recipient of TCS RSP Fellowship (2016-present).

Swades De (S'02-M'04-SM'14) received his B.Tech. in Radiophysics and Electronics from the University of Calcutta, India, in 1993, his M.Tech. in Optoelectronics and Optical Communication from IIT Delhi in 1998, and his Ph.D. in Electrical Engineering from the State University of New York at Buffalo in 2004.

Dr. De is currently a Professor in the Department of Electrical Engineering at IIT Delhi. Before moving to IIT Delhi in 2007, he was a Tenure-Track Assistant Professor of Electrical and Computer Engineering at the New Jersey Institute of Technology (2004-2007). He worked as an ERCIM post-doctoral researcher at ISTI-CNR, Pisa, Italy (2004), and has nearly five years of industry experience in India on telecom hardware and software development (1993-1997, 1999). His research interests are broadly in communication networks, with emphasis on performance modeling and analysis. Current directions include energy harvesting sensor networks, broadband wireless access and routing, cognitive/white-space access networks, smart grid networks, and IoT communications.

Dr. De currently serves as an Area Editor for the IEEE COMMUNICATIONS LETTERS and Elsevier Computer Communications, and an Associate Editor for the IEEE TRANSACTIONS ON VEHICULAR TECHNOLOGY, the IEEE WIRELESS COMMUNICATIONS LETTERS, the IEEE NETWORKING LETTERS, and the IETE Technical Review journal.